Charge radii and nuclear structure

G. B. Krygin and V. E. Mitroshin

B. P. Konstantinov Leningrad Institute of Nuclear Physics, USSR Academy of Sciences, Gatchina
Fiz. Elem. Chastits At. Yadra **16**, 927–965 (July–August 1985)

It is shown that reliable information on the nature of the nuclear forces can be obtained by studying the variation of the mean-square charge radii on excitation of a nucleus as well as on the transition from isotope to isotope. However, the solution of this complicated problem is impossible without an accurate description of the wave-function structure. Therefore, the theoretical analysis of $\Delta\langle r^2\rangle$ is founded on the dynamical collective model, which reproduces well the excitation spectra and all the spectroscopic characteristics of odd nuclei. Systematic calculations of $\Delta\langle r^2\rangle$ in the case of excitation of spherical and transition nuclei from ^{73}Ge to ^{141}Pr and also calculations of the isotopic effects in the mean-square charge radii of mercury and cesium have revealed a number of new dynamical effects. Ways of determining the constants of the nuclear interaction are discussed.

INTRODUCTION

Study of the mean-square charge radii of nuclei and their variations when a nucleus is excited or when nucleons are added has been one of the central themes of nuclear physics in recent years. Whereas the charge radius characterizes the nucleus as a whole, the change in the mean-square charge radii on excitation of a nucleus or on the addition of nucleons is determined by both the nuclear structure and the nature of the effective forces. Let us explain what we mean.

It is convenient to divide the effective forces between nucleons in nuclei into two classes, putting in the first class the forces for which the stability (with respect to collapse) of the single-particle field generated by them is ensured by a strong density dependence (for example, Skyrme-3 forces). In the second class, we put the forces for which the stability of the single-particle field is ensured by a strong velocity dependence (for example, Skyrme-5).

For the forces of the first class, the transfer of density to the surface of the nucleus when it is excited entails a deepening and contraction of the single-particle field.[1] Therefore, the changes in the mean-square charge radii will be minimal. In contrast, for the forces of the second class the transfer of density entails a decrease in the depth of the single-particle field, which becomes wider. Because the single-particle matrix elements increase at the same time, the effect is enhanced still further, and therefore the changes in the mean-square charge radii will be maximal, i.e., will exceed the value $\Delta\langle r^2\rangle$ obtained in the rigid-field approximation. This simple observation makes it possible to get a real grip on the problem of the nature of the effective nuclear forces.

Indeed, suppose that on excitation of a nucleus the single-particle field changes by the amount δV: $\tilde{V} = V + \delta V$. Here and in what follows, the tilde identifies an excited state. Then the change in the single-particle wave functions will be

$$\delta\varphi_j = \tilde{\varphi}_j - \varphi_j \simeq \sum_{j' \neq j} \frac{\langle j|\delta V|j'\rangle}{e_j - e_{j'}}\varphi_{j'}, \qquad (1)$$

where e_j is the energy of the single-particle state. We now find the change in the charge density of the nucleus following its excitation up to small terms of first order:

$$\delta\rho = \sum (n_j + \delta n_j)\ (\varphi_j + \delta\varphi_j)^2 - \sum n_j\varphi_j$$
$$\simeq \sum \delta n_j\varphi_j^2 + 2\sum n_j\varphi_j\delta\varphi_j. \qquad (2)$$

Here, n_j are the population numbers of the single-particle states in the ground state of the nucleus, while $n_j + \delta n_j$ are their values in the excited state.

Thus, the change in the mean-square charge radius of the nucleus following its excitation can be represented as a sum of two terms:

$$Z\Delta\langle r^2\rangle = \int \delta\rho\,(r)\, r^2 d^3r = \Delta_1(\delta n) + \Delta_2(\delta\varphi), \qquad (3)$$

where Z is the number of protons in the nucleus. As can be seen from (3), Δ_1 is associated with structural effects (δn) but Δ_2 with the rearrangement of the single-particle field and, thus, with the nature of the effective nuclear forces.

We assume that the experimental value $\Delta\langle r^2\rangle_{\text{exp}}$ is known with high accuracy. Thus, to solve the problem of the type of the forces, i.e., to find Δ_2,

$$\Delta_2(\delta\varphi) = \Delta\langle r^2\rangle_{\text{exp}} - \Delta_1(\delta n),$$

it is necessary to calculate Δ_1 on the basis of a model that describes accurately the structure of the nuclear states.

The present review is devoted to the calculation of Δ_1 for a large number of nuclei and to the study of the part played by various structural effects, the basis of our considerations being the dynamical collective model (DCM) considered in Sec. 3.

In Sec. 1, we briefly discuss methods of determining $\Delta\langle r^2\rangle$ from experimental Mössbauer data. The literature on this problem is given as fully as possible, and therefore all the details can be reproduced if the reader wishes. Section 2 discusses various theoretical approaches to the study of $\Delta\langle r^2\rangle$, while in Sec. 3 various limiting cases are considered on the basis of the expression obtained in the DCM for the mean-square charge radii. Sections 4 and 5 present the results of systematic calculations of Δ_1 in the case of excitation of spherical and transitional nuclei, and the part played by various dynamical effects is studied. The isotopic effects in the mean-square charge radii are studied in Sec. 6 for the exam-

 0090-4759/85/040410-21$04.40

TABLE I. Experimental $\Delta\langle r^2\rangle$ values obtained by different methods for a number of nuclei.

Nucleus	$\Delta\langle r^2\rangle$, 10^{-3} F^2				
	1	2	3	4	5
^{57}Fe	−14.1 (7)	−11.5	−7.9 (1.3)	−14.3	−11.7
^{83}Kr	–	—	—	6.4	12.8
^{99}Tc	—	—	—	5.5	6.9
^{99}Ru	—	—	12.8	14.2	12.8
^{119}Sn	3.3	—	6.9 (9)	3.3	5.3
^{121}Sb	—	—	—	−24.6	−50.8
^{125}Te	—	—	5.6	2.7	3.3
^{129}I	—	—	—	18.5	13.7
^{129}Xe	—	—	—	1.5	5.4
^{133}Cs	—	—	—	3.8	5.6
^{141}Pr	—	—	—	14.0	8.2

Remark. 1) Frozen-ion method[14–16]; 2) band calculations; 3) measurement of $\Delta\lambda/\lambda$ and internal-conversion coefficient[18,19]; 4) free-ion approximation[20]; 5) extended ratio method.[21]

ple of isotopes of mercury and cesium. The results of these investigations are presented in Sec. 7 and in the Conclusions.

1. EXPERIMENTAL METHODS OF DETERMINING $\Delta\langle r^2\rangle$

The quantity $\Delta\langle r^2\rangle_{\text{exp}}$ corresponding to excitation of a nucleus can be separated from the experimentally observed isomer shift Δv of the Mössbauer lines of the absorber relative to the γ source by means of the well-known expression

$$\Delta v = \frac{2\pi}{3}\frac{cZe^2}{E_\gamma}\Delta\rho(0)\,\Delta\langle r^2\rangle, \qquad (4)$$

where c is the velocity of light, Z is the number of protons in the nucleus, e is the electron charge, E_γ is the energy of the Mössbauer transition, and $\Delta\rho(0)$ is the increment in the total density of the orbital electrons at the position at which the absorber nucleus is situated relative to the source. The determination of $\Delta\langle r^2\rangle$ in accordance with (4) is called isomer-shift calibration. Generally, the experimental error in the measurements of Δv is of the order of a few percent, and therefore the accuracy of the calibration depends directly on the accuracy in the determination of $\Delta\rho(0)$.

The achievements in the isomer-shift calibration are reflected in the reviews published by Goldanskii and Herber,[2] the monograph of Shpinel',[3] and other publications.[4–11] Recently, the number of studies on calibration has sharply increased.[12,13] However, none of the calibration methods can be made universal. In the majority of cases, this is simply impossible, since the experimental methods used for one group of nuclei are either ineffective or completely unsuitable for other nuclei. The absence of a universal and reliable method for calibrating the isomer shifts generated, and still does, contradictory opinions about the values of $\Delta\langle r^2\rangle$ (Table I).[14–21]

It is obvious that the problem of calibrating the isomer shifts would be removed if we could make an exact quantum-mechanical calculation of $\Delta\rho(0)$. As yet, this is impossible, although in recent years much work has been done in this direction. But it should also be pointed out that even knowledge of the exact value of $\Delta\langle r^2\rangle$ for one or two nuclei would not make it possible at the present stage to draw any reliable conclusions about the nature of the effective nuclear forces. We give a characteristic example: At the present time, the energies of excited states are measured in nuclear spectroscopy to an accuracy of fractions of an electron volt. But as yet this yields little for our understanding of real nuclear physics. The problem is the imperfections of the model conceptions of the nuclear system—problems associated with truncation of the basis, parametrization, etc., frequently remain open. It is for this reason that it is important to study a variety of characteristics for as many nuclei as possible in order to establish first a general picture of nuclear dynamics.

The situation with regard to the study of $\Delta\langle r^2\rangle$ is similar. But in this case the situation is aggravated by uncertainty of the experimental data. It therefore appears to us that the attempt to determine the constants of the effective forces is premature. But one can attempt to establish the type of the effective forces by studying the systematics of the differences between $\Delta\langle r^2\rangle_{\text{exp}}$ and Δ_1.

With regard to the isotopic variations of the mean-square charge radii, the experimental methods are in this case not subject to such uncertainty as in the case of the isomer variations of the mean-square charge radii. Genuine progress in the experimental determination of the isomer variations of the mean-square charge radii has come with the wide use of laser spectroscopy and mass separators.[22–26] This has made it possible to obtain data on $\Delta\langle r^2\rangle$ for many isotopes of one element. The results of some experiments of this kind are given in Table II.

2. DESCRIPTION OF $\Delta\langle r^2\rangle$ IN DIFFERENT NUCLEAR MODELS

We now consider the problem of describing the structure of the states and $\Delta\langle r^2\rangle$ in different nuclear models.

The calculations of Refs. 27–30 show that the single-particle approximation and the superfluid model are too crude from the point of view of describing the structure of nuclear states and therefore in the majority of cases even give the incorrect sign of $\Delta\langle r^2\rangle$. This means that allowance for the interaction of an odd nucleon with the core must play an important part. It was proposed in Ref. 31 that the nucleus should be treated as a core plus several valence nucleons. The description of the core is based on the liquid-drop model with allowance for only monopole and quadrupole polariza-

TABLE II. Isotopic variations of $\Delta\langle r^2\rangle$ for the nuclei of Xe, Cs, Ba, and Hg.

N	N'	$\Delta\langle r^2\rangle_{N,N'}$, F^2			N	$\Delta\langle r^2\rangle_{N,124}$, F^2
		Xe	Cs	Ba		Hg
70	72	0.054 (29)	—	—	101	−0.471 (6)
72	74	0.050 (28)	0.051 (30)	—	103	−0.420 (5)
74	75	0.002 (11)	—	—	104	−0.962 (4)
74	76	0.044 (30)	0.065 (23)	0.018 (10)	105	−0.429 (4)
76	77	−0.012 (16)	−0.027 (14)	—	106	−0.881 (4)
76	78	0.035 (32)	−0.007 (13)	0.022 (9)	107	−0.850 (4)
78	79	—	−0.011 (6)	−0.022 (10)	108	−0.800 (4)
78	80	0.042 (29)	0.025 (11)	0.016 (9)	109	−0.782 (4)
80	81	—	0.038 (40)	0.020 (6)	110	−0.711 (4)
70	82	0.283 (99)	—	—	111	−0.698 (5)
72	82	0.229 (30)	0.190 (59)	—		
74	82	0.179 (70)	0.139 (48)	0.101 (40)		
75	82	0.177 (60)	—	—		
76	82	0.135 (60)	0.074 (33)	0.083 (30)		
77	82	0.147 (40)	0.101 (29)	—		
78	82	0.100 (40)	0.081 (22)	0.061 (20)		
79	82	—	0.092 (16)	0.083 (16)		
80	82	0.058 (20)	0.056 (11)	0.045 (10)		
81	82	—	0.018 (40)	0.065 (6)		

tions. The residual forces are chosen in the form of pairing and quadrupole interactions. The resulting wave functions

$$|j\rangle = c_j \overset{+}{\alpha}_j |0\rangle + \sum_i c_i^{(j)} [\overset{+}{\Omega}_\lambda \overset{+}{\alpha}_i]_j |0\rangle,$$

obtained by diagonalization of such a Hamiltonian, are used to calculate the mean-square charge radii. Here, $\overset{+}{\Omega}_\lambda$ and $\overset{+}{\alpha}_j$ are the phonon and quasiparticle creation operators; the vacuum is defined relative to the phonons. To calculate the mean-square charge radii, the effective operator $\hat{R}^2$ was used:

$$\left.\begin{aligned} \hat{R}^2 &= \sum_{ij} \langle j|r^2|i\rangle_{\text{eff}} \overset{+}{a}_j a_i + Z_0 R_c^2(\beta^2); \\ R_c^2(\beta^2) &= R_0^2(1 + (5/4)\pi\beta^2), \end{aligned}\right\} \quad (5)$$

where Z_0 is the number of protons in the core, R_0^2 is the equilibrium radius, β^2 is the mean-square deformation, and the summation is only over the states of the valence nucleons. The effective operator (5) includes monopole polarization of the core:

$$\langle j \mid r^2 \mid i\rangle_{\text{eff}} = \delta_{j,p} \langle j \mid r^2 \mid j\rangle + R_0(\delta_{i,n} - 2Z_0 s_j/K),$$

where K is the rigidity parameter, used in the calculations as a free parameter, and $s_j = \partial e_j/\partial \Delta$ is the change in the energy of the single-particle state corresponding to the change in the rms radius of the core, $\Delta = (R - R_0)/R_0$. The quantities s_j were calculated in a Woods–Saxon potential with four free parameters. Three of them were chosen to match the experimental data on the isotopic shifts and electron scattering, while the fourth together with the rigidity parameter K were chosen directly in the calculation of $\Delta\langle r^2\rangle$. Table III gives some results of the calculations made in Ref. 31 and a comparison with experiment. It can be seen that the calculations are only in qualitative agreement with experiment, this being due to the approximate description of the structure of the states of the odd nuclei in the framework of this model.

The results of the first calculations of $\Delta\langle r^2\rangle$ in the framework of the theory of finite Fermi systems for spherical and transitional nuclei in the single-particle[32] and quasiparticle[33] approximations differ strongly from the experimental values. But in recent years significant successes have been achieved in this direction[34,35] for nuclei in the region of lead, particularly after allowance for the collective degrees of freedom. But the importance of structural effects was most clearly revealed by calculations of $\Delta\langle r^2\rangle$ in the theory of finite Fermi systems for odd deformed nuclei.[36,37] In Ref. 36, the values of the constants of the particle-particle and particle-hole interactions for which the best description of $\Delta\langle r^2\rangle_{\text{exp}}$ for the nuclei from ^{151}Eu to ^{167}Dy was obtained are as follows:

$$f_{in}^{pp} = 1.0, \quad f_{ex}^{pp} = -2.6, \quad f_{in}^{hp} = +0.48, \quad f_{ex}^{hp} = -3.4.$$

However, in Ref. 37 the constants of the effective forces were determined from the description of the muon isomer shifts of the nucleus ^{152}Sm and were found to be 0.8, − 1.5, − 0.8,

TABLE III. Calculated[31] and experimental values of $\Delta\langle r^2\rangle$ resulting from excitation of a number of nuclei.

Nucleus	$\Delta\langle r^2\rangle$, 10^{-3} F^2		Nucleus	$\Delta\langle r^2\rangle$, 10^{-3} F^2	
	Calculation	Experiment		Calculation	Experiment
^{57}Fe	−43.0	−11.7	^{127}I	−1.0	−9.3
^{83}Kr	33.0	12.8	^{129}I	1.3	13.7
^{119}Sn	3.0	5.3	^{133}Cs	1.0	8.3
^{125}Te	−3.0	3.2	^{197}Au	−26.0	16.8

TABLE IV. Changes in the charge as calculated in the theory of a number of deformed nuclei as calculated in the theory of finite Fermi systems.

Nucleus	E, keV	$\Delta\langle r^2\rangle$, 10^{-3} F^2		
		Ref. 36	Ref 37	Experiment
^{151}Eu	22	11.0		11.2
^{153}Eu	97	−50.3	−86.9	−58.3
	103	−57.5	−112.5	−59.9
^{155}Gd	87	−8.4		−5.6
	105	−14.1		−7,7
^{157}Gd	64	14.7		14.3
^{161}Dy	26	42.7		5.8
	75	37.9		6.1

and − 3.33, respectively. It can be seen that the constants differ appreciably. The corresponding description of $\Delta\langle r^2\rangle$ which is then obtained can be seen from Table IV. It can be seen from the comparison that the results of Ref. 36 agree well with experiment. However, the real value of these results can be seen in Fig. 1, which is taken from the same study. It can be seen that even a very small change in δ produces large changes in $\Delta\langle r^2\rangle$. This indicates that exact description of the structure of the states can be a decisive factor. For example, the poor description of $\Delta\langle r^2\rangle$ in ^{153}Eu obtained in Ref. 37 can therefore be due to the poor description of the structure of the states rather than to an unfortunate choice of the constants of the effective forces. For in none of these studies was either a description of the spectra of the investigated nuclei or the spectroscopic characteristics of the states obtained. Moreover, the values of δ chosen by the authors of Ref. 36 differ from the values usually adopted for these nuclei, and the variation in the deformation parameter on excitation of the nucleus, which can occur,[38,39] was not considered at all.

From what we have said it is clearly seen that conclusions about the nature of the effective forces can be justified only if the structural part in $\Delta\langle r^2\rangle$ is separated with the greatest accuracy possible. Therefore, study of $\Delta\langle r^2\rangle$ must be based on a model that most adequately describes all the available experimental information on at least the properties of the low-lying states.

3. STUDY OF $\Delta\langle r^2\rangle$ IN THE DYNAMICAL COLLECTIVE MODEL

From the formal point of view, the DCM[40] is the standard model describing the coupling of an odd quasiparticle to the collective excitations of a spherical core. But it differs from such models in taking into account the effect of the Pauli principle[41] and the zero-point shape vibrations[42] on the formation of the single-particle and collective degrees of freedom and their coupling. Among all the collective excitations of the core, allowance is made for only the yrast state band, for the description of which the dynamical version of the generalized collective model[43] is used.

The wave function of the state of an odd nucleus with total angular momentum I^π is sought in the form of the expansion

$$|I^\pi\rangle = \sum_{jR} F_{jR}^{(I)} D_j\, |(jR)_I\rangle$$

with respect to all possible states $|j\rangle$ of the odd quasiparticle and the core $|R\rangle$ allowed by the conservation laws for the total angular momentum and parity. However, in the DCM one uses the f_{jK} representation,[44] which is unitarily equivalent to F_{jR}:

$$f_{jK}^{(I)} = \sqrt{2} \sum_{R=0,\,2\ldots} [2R+1]^{1/2} \begin{pmatrix} j & R & I \\ -K & 0 & K \end{pmatrix} F_{jR}^{(I)},$$

where the f_{jK} amplitudes have the same symmetry properties as the amplitudes in the expansion of the total wave function with respect to the states of the "rotator–particle" model. This is convenient, on the one hand, for comparison with results of calculations in the cranking model and, on the other, makes it possible to represent the results of the calculations clearly, the cranking model being obtained in the DCM in the limit of classical mechanics.

The mean value of the total Hamiltonian in the f_{jK} representation has the form

$$\langle I|H_{\text{tot}}|I\rangle = \sum_{jKj'K'} \left\{ \left[\varepsilon_j \delta_{KK'} + 2 \sum_{R=0,\,2,\,\ldots} (E_R + \delta E_{jR}^I)\,(2R+1) \right.\right.$$

$$\times \left.\left. \begin{pmatrix} j & R & I \\ -K & 0 & K \end{pmatrix} \begin{pmatrix} j & R & I \\ -K' & 0 & K' \end{pmatrix} \right] \delta_{jj'} - \tilde{Q}_{jj'}^{(-2,\,2)} \cdot 2 \sum_{R,\,R'} [(2R+1) \right.$$

$$\times (2R'+1)]^{1/2} \begin{pmatrix} j & R & I \\ -K & 0 & K \end{pmatrix} \begin{pmatrix} j' & R' & I \\ K' & 0 & -K' \end{pmatrix}$$

$$\left. \times \begin{Bmatrix} j' & R' & I \\ R & j & 2 \end{Bmatrix} G_2^{(R,\,R')} \right\} f_{jK}^{(I)} f_{j'K'}^{(I)}, \qquad (6)$$

and technically the problem reduces to finding amplitudes f_{jK} that reduce the matrix in the curly brackets to diagonal form. We shall describe the quantities that occur in (6):

E_R, the energy of the excited state of the core with mo-

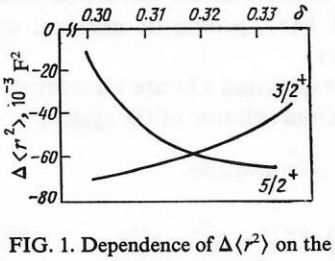

FIG. 1. Dependence of $\Delta\langle r^2\rangle$ on the deformation parameter δ.

ment R, is equal to

$$E_R = R\omega_R^{(2)}/2 + 5/2\,(\omega_R^{(2)} - \omega_2^{(2)});\quad \omega_R^{(2)} = E\,(2_1^+)\sqrt{1+\gamma\,(R-2)}.$$

Here, γ is a coefficient that reflects the part played by the Pauli principle in forming the collective modes; it can be calculated either from the description of the yrast band or in accordance with the formula

$$\gamma = \tilde{\gamma}\,(1+\omega_{\text{coul}}^2/\omega_2^{(2)2});\quad \omega_{\text{coul}}^2 = 3e^2Z^2/(10\pi R_0 B_2);$$
$$\tilde{\gamma} = (5.5 - 0.002\,A)\,10^{-2};\quad 40 \leqslant A \leqslant 150,$$

where B_2 is the mass parameter expressed in terms of B ($E2$, $0_1^+ \to 2_1^+$) in the standard manner.

The collective matrix elements $G_{\lambda=2}^{(R,R')}$ are equal to

$$G_\lambda^{(R,R')} = G_2^{(0,2)}\,[(2R+1)/5]^{1/2}$$
$$\times \begin{cases} \rho_R^{1/2}, & R \neq R'; \\ \varkappa\left[\dfrac{5+R}{\sqrt{1+\gamma\,(R-2)}} - \rho_R - \dfrac{2R+5}{2R+1}\,\rho_{R+2}\right]^{1/2}, & R = R', \end{cases}$$

where

$$G_2^{(0,2)} = \left[\frac{5}{2B_2E\,(2_1^+)}\right]^{1/2},$$

$$\rho_R = \frac{R}{2}\,\frac{1-\gamma}{1+\gamma\,(R-4)}\left[1 - \frac{\gamma}{2\,(1+\gamma\,(R-2))}\right]^{(R-2)/2},$$

and the constant $\varkappa$ is expressed in terms of the quadrupole moment of the 2_1^+ state as follows:

$$Q\,(2_1^+) = 3/4\pi Z R_0^2 G_2^{(2,2)}.$$

In the expression (6), δE_{jR}^I is the correction for the noncommutativity of the collective and single-particle modes calculated in the approximation that the state $|R\rangle$ corresponds to a pure N-phonon state with moment $R = N\lambda$:

$$\delta E_{jR}^I = \frac{R}{\lambda}\left[\delta\omega_{jR}^I|_{\omega_R} + \frac{d}{d\omega}\,(\delta\omega_{jR}^I)|_{\omega_R}\,\delta\omega_{jR}^I|_{\omega_R} + \ldots\right],$$

where

$$\delta\omega_{jR}^I = -[2\,(2\lambda+1)\,B_\lambda\omega_R^{(\lambda)}]^{-1}\sum_{j'}\frac{q_{jj'}^{(\lambda)2}\,(u_jv_{j'}+v_ju_{j'})^2}{\varepsilon_j+\varepsilon_{j'}-\omega_R^{(\lambda)}}$$
$$\times\,(1-\eta_j^{(R)}-\eta_{j'}^{(R)})\,(2\lambda+1)\sum_J(2R+1)\,(2J+1)$$
$$\times\begin{Bmatrix} I & j & R \\ \lambda & R-\lambda & J\end{Bmatrix}^2\begin{Bmatrix}\lambda & j & j'\\ \lambda & j & J\end{Bmatrix}. \qquad (7)$$

Here u_j, v_j, and ε_j are the superfluidity coefficients and the quasiparticle energy in the single-particle state j, calculated from the solution of the standard superfluidity equations (see below), and

$$q_{jj'}^{(\lambda)} = \left\langle j\left\|r\,\frac{dV(r)}{dr}\,Y_\lambda\right\|j'\right\rangle$$

is the single-particle reduced matrix element calculated with the single-particle potential $V(r)$, proton or neutron, to which the indices j and j' refer.

The numbers η_j in the expression (7) are vacuum expectation values, calculated from solution of the system

$$\eta_j^{(R)} = (2j+1)^{-1}\sum_m\langle 0|\overset{+}{\alpha}_{jm}\alpha_{jm}|0\rangle$$
$$= \sum_{\Lambda=2,3\ldots}\frac{2\Lambda+1}{2j+1}\sum_{j'}s_{jj'}^{(\Lambda,R)2}\,(1-\eta_j^{(R)}-\eta_{j'}^{(R)}), \qquad (8)$$

where $s_{jj'}^{(\Lambda,R)}$ (respectively, $r_{jj'}^{(\Lambda,R)}$) are the amplitudes of annihilation to the vacuum or creation from the vacuum of a pair of quasiparticles and a phonon of multipolarity Λ in the N-phonon state with moment $R = N\Lambda$ (and, respectively, the amplitude of annihilation of a pair of quasiparticles into a phonon); they are calculated in accordance with

$$\left.\begin{matrix} r_{jj'}^{(\Lambda,R)} \\ s_{jj'}^{(\Lambda,R)}\end{matrix}\right\} = [2\,(2\Lambda+1)\,B_\Lambda\omega_R^{(\Lambda)}]^{-1/2}\,\frac{q_{jj'}^{(\Lambda)}\,(u_jv_{j'}+v_ju_{j'})}{\varepsilon_j+\varepsilon_{j'}\mp\omega_R^{(\Lambda)}}. \qquad (9)$$

In the expression (6), the matrix element $\tilde{Q}_{jj'}^{(-2,2)}$ is the matrix element $Q_{jj'}^{(-2)} = q_{jj'}^{(2)}\,(u_ju_{j'} - v_jv_{j'})$ renormalized by the effect of the zero-point shape vibrations. Both here and in the calculation of other single-particle moments the renormalized Q moments are determined from the solution of the equation

$$\tilde{Q}_{jj'}^{(\pm\lambda,R)} = D_jD_{j'}\Bigg[Q_{jj'}^{(\pm\lambda)}\,(1-\eta_j^{(R)}-\eta_{j'}^{(R)}) + \sum_{\substack{\Lambda=2,3\ldots\\ i,\,i'}}(2\Lambda+1)$$
$$\times\,(-1)^{i\mp i'+\lambda+1}\,s_{ji}^{(\Lambda,R)}\tilde{Q}_{ii'}^{(\pm\lambda,R)}s_{i'j'}^{(\Lambda,R)}\,(1-\eta_j^{(R)}-\eta_i^{(R)})$$
$$\times\,(1-\eta_{i'}^{(R)}-\eta_{j'}^{(R)})\begin{Bmatrix} i & i' & R\\ j' & j & \Lambda\end{Bmatrix}\Bigg], \qquad (10)$$

where $Q_{ii'}^{(\pm\lambda)}$ is the unrenormalized moment multiplied by the superfluid factor $V_{jj'}^{(\pm)} = u_ju_{j'} \pm v_jv_{j'}$, and the signs $\pm$ correspond to the T-odd and T-even operators, respectively. In the renormalization calculations in accordance with (10) an important part is sometimes played by not only the quadrupole zero-point shape vibrations, $\Lambda = 2$, but also by the octupole $\Lambda = 3$. The mass parameter for them was determined in the standard manner in terms of B_2, and the 3_1^- state energy, if its experimental value was not known, was calculated by the method of Ref. 45.

To calculate the probabilities of radiative transitions, the operator $\mathfrak{M}(F\lambda)$ responsible for the electric and magnetic transitions is represented as a sum of the contributions of single-particle and collective parts[46]:

$$\mathfrak{M}(F\lambda) = \mathfrak{M}_{\text{sp}}(F\lambda) + \mathfrak{M}_{\text{col}}(F\lambda).$$

Thus, for $E2$ transitions

$$\mathfrak{M}_{\text{sp}}(E2) = e^{\text{eff}}r^2Y_{2\mu},\quad \mathfrak{M}_{\text{col}}(E2) = 3/4\pi eZR_0^2\alpha_{\lambda\mu}$$
$$e^{\text{eff}} = \begin{cases} 1+Z/A^2 & \text{for protons,}\\ Z/A^2 & \text{for neutrons.}\end{cases}$$

For the $M1$ moments

$$\mathfrak{M}_{\text{sp}}(M1) = \mu\,[(g_s - g_p)\,\mathbf{s} + g_l\mathbf{j}],$$

$$\mathfrak{M}_{\text{col}}(M1) = \mu g_R\mathbf{R},\quad g_R = Z/A,$$

$$g_s = \begin{cases} +5{,}58\\ -3{,}82\end{cases},\quad g_l = \begin{cases} 1 & \text{for protons,}\\ 0 & \text{for neutrons.}\end{cases}$$

The matrix elements of the operator $\mathfrak{M}$ are calculated in the approximation of commutativity of the collective and single-particle modes, but in the calculation of the matrix elements of the single-particle part of the operator the renormalization in accordance with (10) due to the influence of the zero-point shape vibrations is taken into account.

The spectroscopic amplitudes are also calculated with

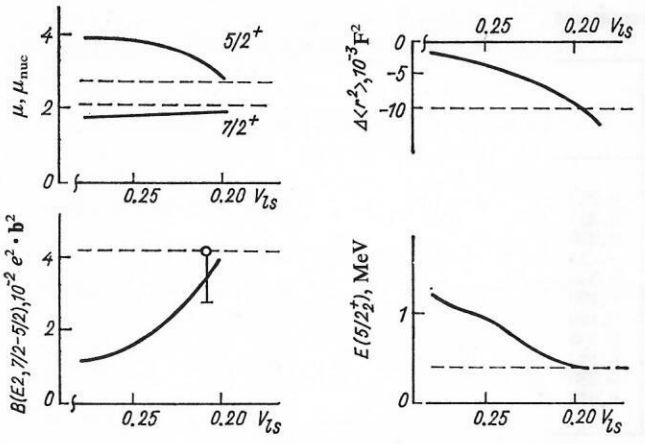

FIG. 2. Dependence of the spectroscopic characteristics and $\Delta\langle r^2\rangle$ on the constant V_{ls} of the spin-orbit forces (the broken line represents the experiment).

allowance for the influence of the zero-point shape vibrations:

$$
\begin{aligned}
{}_n\langle jm|\overset{+}{a}_{jm}|0\rangle = {} & D_j F_{j0}^{(j)} u_j (1-\eta_j^{(0)}) + v_j \left[\frac{2\lambda+1}{2j+1}\right]^{1/2} \sum_{j_1} D_{j_1} F_{j_1 2}^{(j)} \\
& \times (1-\eta_j^{(2)}-\eta_{j_1}^{(2)})\, s_{jj_1}^{(2,\,2)} \\
& + \sqrt{2}\, u_j \sum_{j_1 j_2} D_{j_2} F_{j_2 4}^{(j)} (2\lambda+1)\,[9/(2j+1)]^{1/2} \\
& \times \begin{Bmatrix} j & j_2 & R \\ \lambda & \lambda & j_1 \end{Bmatrix} (1-\eta_{j_1}^{(4)}-\eta_{j_2}^{(4)})\, r_{jj_1}^{(2,\,4)} s_{j_1 j_2}^{(2,\,4)}.
\end{aligned}
$$

Here, $\lambda = 2$, and n is the number of the solution (6) with $I = j$.

Parametrization

As can be seen from the expressions (6)–(10), to describe the collective part of the spectrum it is necessary to specify the values of $E(2_1^+)$, B_2, and $\varkappa$, which are taken when possible from experimental data. In calculations of the excitation spectra one allows for B_2 and $\varkappa$ variations within limits such that the calculated $B(E2,\ 0_1^+ \to 2_1^+)$ and $Q(2_1^+)$ differ from the experimental values by not more than three experimental errors (confidence limit). The spectrum of the single-particle states was calculated with a Woods–Saxon potential with the following parameters for the depth V_0, 50% decrease radius, and diffuseness:

$$V_0 = 52.1\left[1+0.647\,\frac{N-Z}{A}\,2\tau\right], \quad R_0 = 1.25A^{1/3}, \quad a = 0.65.$$

The parameters were fixed from the description *on the average* of the following characteristics of a group of nuclei: binding energy and separation energy and their isotopic dependences, and also the charge and mass distributions and their diffuseness. The least certain characteristic of the average field is the constant of the spin–orbit forces,

$$\mathscr{V} = V_{ls}\left[1+2\,\frac{N-Z}{A}\right] V_0/2,$$

which differs even for magic nuclei, to say nothing of other nuclei, for which, in general, it is not known. Therefore, it must be chosen from the condition of best description of the excitation spectrum of an odd nucleus. All that is worth doing in fact is to make the sum $\mathscr{V}^p + \mathscr{V}^n$ approximately constant over the complete periodic table, as follows from the relativistic theory of spin–orbit forces.

Both in the solution of the superfluidity equations and in the description of the excitation spectra and other characteristics, allowance was made for all the single-particle states in the interval from -25 to $+$ (5–10) MeV. With this basis and constant of the pairing forces

$$G = \begin{cases} 20.0/A & \text{for protons,} \\ 17.5/A & \text{for neutrons} \end{cases}$$

a good description of the even–odd mass difference of a large number of nuclei is obtained. At the same time, up to 95% of all the vacuum η amplitudes is exhausted. In the calculations of $E2$ transitions and quadrupole moments of the states, no effective charges were introduced, while in the calculations of the $M1$ transitions and the magnetic moments the spin factor g_s was taken to be equal to 0.8 of the value for a free nucleon in accordance with the data of Refs. 47 and 48 on its renormalization due to spin–spin forces and pion degrees of freedom.

Accuracy of the description of the structure of states of odd nuclei

Taking the most striking and characteristic examples, we now demonstrate the possibilities of the DCM from the point of view of describing the structure of states of odd nuclei and, therefore, its suitability for describing the structural part of the effect of the change in the mean-square charge radii of nuclei following their excitation.

The accuracy in the description of the structure of the states can be gauged by the success with which the spectrum of excited states and the complete set of spectroscopic characteristics are reproduced.

Figure 2 shows the dependence of a number of calculated and experimental characteristics of the nucleus ^{127}I on the constant V_{ls} of the spin–orbit forces. It can be seen that when V_{ls} is reduced all the spectroscopic characteristics approach the experimental values, and one reasonable description of the complete data can be obtained for one definite value of V_{ls}. Such a situation is also observed in other nuclei. It is important to note that in the nucleus ^{127}I, for example, the value of V_{ls} can be fixed by the magnetic moment of the $5/2_1^+$ state, which for $V_{ls} \sim 0.200$ becomes equal to the experimental value but with further decrease in V_{ls} rapidly decreases.

In other nuclei one can also find a characteristic that is the most informative. For example, in the nuclei ^{125}Te and ^{129}Xe it is the quadrupole moment of the $3/2_1^+$ state, whose value can be described only for $V_{ls} = 0.330$. For other V_{ls} one obtains what at the first glance appears to be a reasonable description of the spectra and some spectroscopic characteristics, but one can speak of a correct description of the state structure only when all the data are reproduced. It should be noted that for the standard value $V_{ls} = 0.287$ the

TABLE V. Experimental and calculated values of the collective parameters and constants of the spin–orbit forces.

Nucleus	Core	$Q(2_1^+)$, $e\cdot b$		$B(E2, 0-2)$, $10^{-1}\ e^2\cdot b^2$		V_{ls}
		Calculation	Experiment	Calculation	Experiment	
^{83}Kr	^{82}Kr	−0.062	—	2,06	1,80 (10)	0.260
^{99}Tc	^{98}Mo	−0.294	−0,20 (9)	2,95	2,66 (30)	0.200
^{119}Sn	^{118}Sn	−0.056	−0,05 (14)	2,56	2,30 (27)	0.255
^{121}Sb	^{120}Sn	−0,124	−0.05 (10)	2,72	2,20 (22)	0.235
^{125}Te	^{124}Te	−0,140	−0.11 (10)	5.12	6.0 (1,2)	0.335
^{127}I	^{126}Te	−0,150	−0.20 (9)	5.80	5,32 (37)	0.190
^{129}I	^{128}Te	−0.176	−0.24 (8)	4.64	4,12 (33)	0.190
^{129}Xe	^{128}Xe	−0.235	—	6.84	6.5 (2,5)	0.335
^{133}Cs	^{132}Xe	−0.193	—	3,93	4,4 (3)	0.190
^{139}La	^{138}Ba	−0.061	−0,07 (15)	2,73	3.8 (1,1)	0.230
^{141}Pr	^{140}Ce	−0.110	—	2.16	3,15 (50)	0.310

magnetic moments can be described by reducing the spin factor g_s to 0.6 of the free-proton value, the probabilities of $E2$ transitions by choosing the effective proton charge as a free adjustable parameter, and the energies of the $5/2_2^+$ levels in ^{127,129}I by adjusting the coupling constant. All this indicates that for models in which there are many free parameters the Fermi surface remains undetermined and the separation of the structural part of the change in the mean-square charge radii becomes impossible. The DCM used in the present calculations does not contain such parameters, and the recovery of the shape of the Fermi surface from the description of the spectroscopic characteristics makes it possible to predict the value of $\Delta\langle r^2\rangle$.

The spin–orbit constants determined in this manner and the values of $Q(2_1^+)$ and $B(E2, 0_1^+ \to 2_1^+)$ adopted in the calculations for the nuclei studied in what follows are given and compared with experiment in Table V. The spectra that are then obtained are shown in Fig. 3 in comparison with the experimental ones. It can be seen from the comparison that the calculations reproduce well the picture of the low-lying states and reproduce all the main trends. Further, Table VI, for the isotopes ^{99}Tc and ^{125}Te, shows how one can then describe the known spectroscopic characteristics. The results of the calculations for the other nuclei are like those given in Table VI; they can be found in Ref. 49. Examination of these tables reveals some systematic discrepancies in the description of the experimental data:

a) The calculated probabilities of l-forbidden transitions of $M1$ type are systematically smaller than the experimental values. The calculated probabilities of a number of $E2$ transitions with $\Delta l = 2$ systematically exceed the experimental values by an order of magnitude. Analysis showed that these discrepancies are due to the large effect of antisymmetrization on these transitions.

b) The calculated magnetic moments of odd-neutron nuclei, in contrast to odd-proton nuclei, are systematically above the experimental values in absolute magnitude. This indicates that the renormalization of the g_s factor for neutrons is not the same as the one for protons.

But the listed factors are in no way related to $\Delta\langle r^2\rangle$. And the good description of all the other experimental data guarantees a fairly high accuracy in the calculation of the structural part of $\Delta\langle r^2\rangle$.

Calculation of mean-square charge radii of odd nuclei

Our task is to calculate the diagonal matrix elements of the operator

$$\hat{R}^2 = Z^{-1} \sum_{n,\, n',\, ljm} \langle jln \mid r^2 \mid jln' \rangle \overset{+}{a}_{jm} a_{jm}, \tag{11}$$

where Z is the number of protons in the nucleus, $\overset{+}{a}_{jm}$ is the particle creation operator, and $\langle nlj|r^2|n'lj\rangle$ are the single-particle radial integrals. In operator form, the wave function of the state M with angular momentum I^π has the form

$$|\, I_M\rangle = \sum_{jmR\Omega} F_{jR}^{(I_M)} D_j C_{jmR\Omega}^{IM} \overset{+}{\alpha}_{jm} \overset{+}{R}_\Omega \mid 0\rangle. \tag{12}$$

Here, F_{jR} are expansion amplitudes (in what follows, for brevity, the index I_M is omitted), $C_{jmR\,\Omega}^{IM}$ are Clebsch–Gordan coefficients, and $\overset{+}{\alpha}_{jm}$ are quasiparticle creation operators. The charge radius is calculated in the approximation in which the operator $\overset{+}{R}$ is

$$R^+ = (N!)^{-1/2} [\overset{+}{\Omega}_\lambda [\overset{+}{\Omega}_\lambda \ldots [\overset{+}{\Omega}_\lambda \overset{+}{\Omega}_\lambda]_{2\lambda} \ldots]_{R=N\lambda},$$

the operator of creation of an aligned N-phonon configuration, $\overset{+}{\Omega}_{\lambda\mu}$ being the phonon creation operator. The vacuum is defined relative to the phonons.

Going over in (11) from the fermion operators $\overset{+}{a}$ and a to the quasiparticle operators $\overset{+}{\alpha}$ and α by Bogolyubov transformations, and finding the expectation value of (11) with respect to (12), we obtain

$$\begin{aligned}\langle I \mid \hat{R}^2 \mid I\rangle = {} & Z^{-1} \sum (2j+1)\, v_j^2 \langle j \mid r^2 \mid j\rangle + Z^{-1} \sum F_{i'R'} D_{i'} \\ & \times F_{iR} D_i Q_{jj'} C_{i'n'R'\Omega}^{IM} C_{inR\Omega}^{IM} \langle 0 \mid R'_{\Omega'} \alpha_{i'n'} \overset{+}{\alpha}_{jm} \alpha_{j'm} \overset{+}{\alpha}_{in} \overset{+}{R}_\Omega \mid 0\rangle \\ & + Z^{-1} \sum (-1)^{j-m} F_{i'R'} D_{i'} F_{iR} D_i C_{i'n'R'\Omega}^{IM} C_{inR\Omega}^{IM} \langle j \mid r^2 \mid j'\rangle \\ & \times (\langle 0 \mid R'_{\Omega'} \alpha_{i'n'} \overset{+}{\alpha}_{jm} \overset{+}{\alpha}_{j'-m} \overset{+}{\alpha}_{in} \overset{+}{R}_\Omega \mid 0\rangle\, u_j v_{j'} \\ & + \langle 0 \mid R'_{\Omega'} \alpha_{i'n'} \alpha_{j-m} \alpha_{j'm} \overset{+}{\alpha}_{in} \overset{+}{R}_\Omega \mid 0\rangle\, v_j u_{j'}). \end{aligned} \tag{13}$$

Here, $Q_{jj'} = (u_j u_{j'} - v_j v_{j'})\, \langle j|r^2|j'\rangle$, and by the symbol j' we understand the state with angular momentum equal to j with, however, principal quantum numbers that may differ. To calculate the matrix elements that occur in (13), we must reduce them to "normal" form with respect to the quasipar-

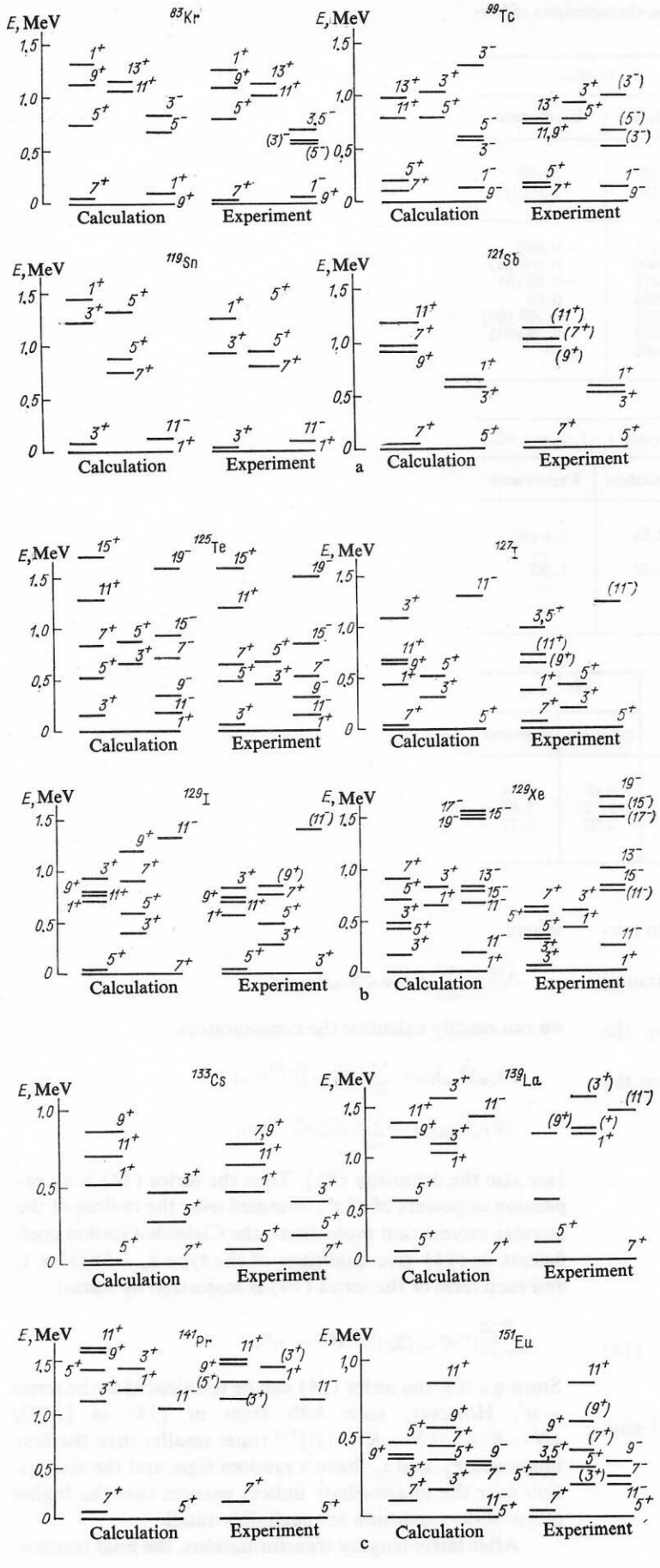

FIG. 3. Calculated and experimental spectra of ^{73}Kr–^{151}Eu. The spin values have been doubled.

TABLE VI. Experimental and calculated values of spectroscopic characteristics of low-lying states of ^{99}Tc and ^{125}Te.

Nucleus	I^π	Q, e·b		μ, μ_{nuc}	
		Calculation	Experiment	Calculation	Experiment
^{99}Tc	$9/2^+$	−0.575	0.34 (34)	5.757	5.685
	$7/2^+$	−0.146	—	4.756	3.6 (9)
^{125}Te	$1/2^+$	0	—	−1.301	−0.888
	$3/2_1^+$	−0.260	−0.31 (2)	0.806	0.604 (5)
	$11/2^-$	0.080	—	−1.212	−0.93 (5)
	$9/2^-$	0.099	0.12	−0.924	−0.66
	$3/2_2^+$	−0.056	—	0.781	0.585 (90)
	$5/2^+$	0.272	—	0.823	0.79 (30)
	$7/2^-$	−0.125	—	−0.464	<0

^{99}Tc

I_i^+	I_f^+	$B(E2,\ I_i - I_f)$, 10^{-1} e^2·b^2		$B(M1,\ I_i - I_f)$, 10^{-2} μ_{nuc}^2	
		Calculation	Experiment	Calculation	Experiment
7/2	9/2	1.04	1.35 (15)	2.64	7.6 (9)
$5/2_1$	9/2	0.58	0.45 (5)	—	—
$5/2_1$	7/2	0.098	—	1.23	1.30
$5/2_2$	9/2	3.18	2.00 (25)	—	—
13/2	9/2	3.64	1.12	—	—

^{125}Te

I_i^+	I_f^+	$B(E2,\ I_i - I_f)$, 10^{-2} e^2·b^2		I^π	$(2I+1)\,S_I$	
		Calculation	Experiment		Calculation	Experiment
1/2	$3/2_2$	0.153	0.186 (5)	$1/2^+$	0.60	0.84
1/2	$5/2_1$	0.180	0.158 (5)	$3/2^+$	1.72	1.84
1/2	$5/2_2$	0.101	0.130	$11/2^-$	3.97	3.72

ticle operators $\overset{+}{\alpha}$ and $\overset{+}{R}$. In reducing the form (13) to normal form in the operators $\overset{+}{R}$, we shall encounter commutators of the type $\left[\overset{+}{\alpha R}\right]_{(-)}$ and $\left[\overset{+}{\alpha}\overset{+}{R}\right]_{(-)}$. Using the definition of $\overset{+}{R}$, we can express these commutators in the form of a series:

$$[\alpha_{jm}\overset{+}{R}{}^{(0)}_{\Omega}]_{(-)} = \sqrt{N}\sum [\alpha_{jm}\overset{+}{\Omega}_{\lambda\mu_1}]_{(-)}\overset{+}{R}{}^{(1)}_{\Omega_1}C^{R_0\Omega_0}_{\lambda\mu_1 R_1\Omega_1}$$
$$+\left[\frac{N-1}{N}\right]^{1/2}\sum [\overset{+}{\Omega}_{\lambda\mu_1}[\alpha_{jm}\overset{+}{\Omega}_{\lambda\mu_2}]_{(-)}]_{(-)}\overset{+}{R}{}^{(2)}_{\Omega_2}C^{R_0\Omega_0}_{\lambda\mu_1 R_1\Omega_1}$$
$$\times C^{R_1\Omega_1}_{\lambda\mu_2 R_2\Omega_2}+\ldots=\sum_{K=1}^{N}\left[\frac{(N-K+1)\,(N-K+1)!}{N!}\right]^{1/2}$$
$$\times\sum [\ldots[\alpha_{jm}\overset{+}{\Omega}_{\lambda\mu_K}]_{(-)}\ldots]_{(-)}\overset{+}{R}{}^{(K)}_{\Omega_K}\prod_{i=1}^{K}C^{R_{i-1}\Omega_{i-1}}_{\lambda\mu_i R_i\Omega_i}. \qquad (14)$$

The series for the commutator $\left[\overset{+}{\alpha}\overset{+}{R}\right]_{(-)}$ is similar. Using the definition

$$\overset{+}{\Omega}_{\lambda\mu}=\frac{1}{2}\sum_{jj'}\{r^{(\lambda,\,R)}_{jj'}\overset{+}{A}{}^{\lambda\mu}_{jj'}-(-1)^{\lambda-\mu}s^{(\lambda,\,R)}_{jj'}A^{\lambda-\mu}_{jj'}\},$$

where

$$\overset{+}{A}{}^{\lambda\mu}_{jj'}=\sum_{mm'}C^{\lambda\mu}_{jmj'm'}\overset{+}{\alpha}_{jm}\overset{+}{\alpha}_{j'm'},$$

we can readily calculate the commutators

$$[\alpha_{jm}\overset{+}{\Omega}_{\lambda\mu}]_{(-)}=\sum_{in}C^{\lambda\mu}_{jmin}r^{(\lambda,\,R)}_{ji}\overset{+}{\alpha}_{in};$$
$$[\overset{+}{\alpha}_{jm}\overset{+}{\Omega}_{\lambda\mu}]_{(-)}=\sum_{in}C^{\lambda-\mu}_{jmin}s^{(\lambda,\,R)}_{ji}\alpha_{in}$$

[see also the definition (9)]. Then the series (14) is an expansion in powers of $r^m s^n$. Summed over the indices of the angular-momentum projections, the Clebsch–Gordan coefficients in (14) give quantities of the type $g_n \sim \{6j\}^2 \ll 1$, and each term of the series (14) is majorized by terms:

$$g^{\frac{m+n}{2}}_{m+n}r^m s^n \leqslant (2g)^{K/2}\,s^{2K}\sim\eta^K.$$

Since $\eta<0.5$, the series (14) can be terminated at the terms $\sim\eta^2$. However, each k-th term in (14) is $[NN!/(N-K+1)(N-K+1)!]^{1/2}$ times smaller than the first; moreover, $r_{jj'}$ and $s_{jj'}$ have a random sign, and the summation over the intermediate indices ensures that the higher terms of the expansion are negligibly small.

After fairly lengthy transformations, the final result is

$$\langle I \mid \hat{R}^2 \mid I\rangle = Z^{-1}\Big\{\sum (2j+1)\, v_j^2\,(1-2\eta_j)\,\langle j \mid r^2 \mid j\rangle$$

$$+\sum (2j+1)\,\eta_j\,\langle j \mid r^2 \mid j\rangle + \sum F_{jR}F_{j'R'}D_jD_{j'}Q_{jj'}\,(1-\eta_j-\eta_{j'})$$

$$-\sum \frac{2\lambda+1}{2j+1}\,F_{jR}F_{j'R'}D_jD_{j'}\,(1-\eta_j-\eta_{i'})\,(1-\eta_{j'}-\eta_i)$$

$$\times Q_{ii'}s_{ji'}s_{j'i}$$

$$+\sum \frac{R}{\lambda}\,F_{iR}^2D_i^2\,(1-\eta_j-\eta_k)\,Q_{jj'}\,(r_{j'k}r_{jk}+s_{j'k}s_{jk})$$

$$+\sum \frac{R}{\lambda}\,(2\lambda+1)\,(2R+1)$$

$$\times\, F_{iR}F_{kR}D_iD_k\,(1-\eta_j-\eta_k)\,(1-\eta_{j'}-\eta_i)\,Q^1_{jj'}$$

$$\times \begin{Bmatrix} I & i & R \\ \lambda & R-\lambda & J \end{Bmatrix} \begin{Bmatrix} I & k & R \\ \lambda & R-\lambda & J \end{Bmatrix}$$

$$\times \left[(2J+1)\begin{Bmatrix} \lambda & i & j \\ \lambda & k & J \end{Bmatrix} r_{kj}r_{ij'} - s_{kj}s_{ij'}\delta_{Jj}\right]$$

$$+\sum \frac{R}{\lambda}\,(2\lambda+1)\,(2R+1)\,F_{iR}F_{jR}D_iD_j\,(2-2\eta_k-\eta_{j'}-\eta_i)\,Q_{jj'}$$

$$\times \begin{Bmatrix} I & j & R \\ \lambda & R-\lambda & J \end{Bmatrix} \begin{Bmatrix} I & i & R \\ \lambda & R-\lambda & J \end{Bmatrix}$$

$$\times \left[(2J+1)\begin{Bmatrix} \lambda & j & k \\ \lambda & i & J \end{Bmatrix} r_{ik}r_{j'k} - s_{ik}s_{j'k}\delta_{J,\,k}\right]$$

$$+\sum 2\left[\frac{R}{\lambda}\,(2\lambda+1)\,(2R+1)\right]^{1/2}$$

$$\times\, D_iD_j\,(1-\eta_j)\,(1-\eta_j-\eta_i)\,(u_jv_{j'}+v_ju_{j'})$$

$$\times\langle j \mid r^2 \mid j'\rangle\left[(-1)^{i-I}\,F_{jR}F_{iR-\lambda}r_{jj'}\begin{Bmatrix} I & j & R \\ \lambda & R-\lambda & i \end{Bmatrix}\right.$$

$$\left.+(-1)^{j-I}\,F_{iR}F_{jR-\lambda}s_{ij'}\begin{Bmatrix} I & i & R \\ \lambda & R-\lambda & j \end{Bmatrix}\right]\Big\}. \qquad (15)$$

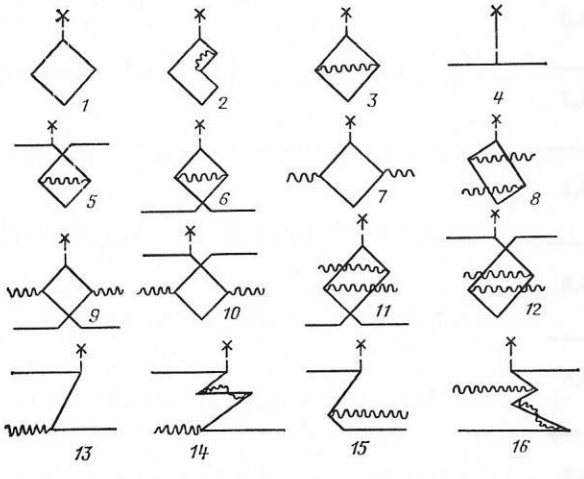

FIG. 4. Classes of diagrams taken into account in calculations of the mean-square charge radii.

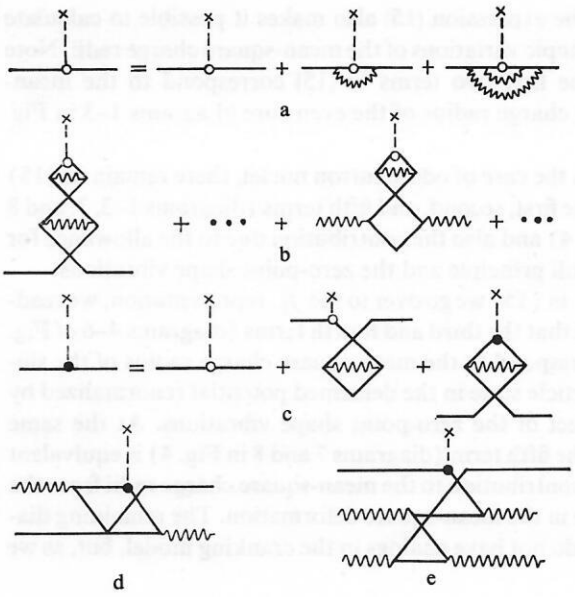

FIG. 5. Commentaries on classes of diagrams taken into account in the calculations (explanations in the text).

In the diagrammatic representation, the expression (15) corresponds to allowance for the processes shown in Fig. 4. Note that by each line of a quasiparticle we understand its fragmentation due to coupling to the collective modes and, for example, diagram 4 in Fig. 4 represents the set shown in Fig. 5a. It must, however, be borne in mind that in the sequence of diagrams shown in Fig. 4 no allowance is made for higher correlation diagrams, for example, as in Fig. 5b. To take into account the complete sequence of diagrams, it is necessary to find the matrix element $Q_{jj'}$ from the solution of the integral equation (10) (its diagrammatic representation is shown in Fig. 5c), and then in the terms containing Q to replace $Q_{jj'}$ by $\tilde{Q}_{jj'}$, ignoring at the same time the fourth term in (15).

Diagrams 9–16 in Fig. 4 describe only the static part of the effect of the Pauli principle. It is also necessary to take into account the dynamical part associated with the change in the frequency of the collective modes. For this, the phonon amplitudes and the η numbers must be expanded in powers of $\delta\omega$ near the unperturbed solution ω_R. For example, for the amplitudes η_j we have

$$\eta_j(\omega) = \eta_j(\omega_R) + \frac{\partial}{\partial\omega}\,\eta_j\delta\omega^I_{j_0R}\Big|_{\omega=\omega_R} + \ldots,$$

where the frequency shift due to the Pauli principle between the odd quasiparticle in the state j_0 and the phonon is determined by the expression (7). In the present work, the terms were calculated up to the second derivative, this corresponding, for example, to allowance for the diagrams shown in Fig. 5d and more complicated ones. Allowance for the effect of the Pauli principle between the N-phonon configurations results in a growth of the oscillator frequency $\omega_R^{(\lambda)} = E(2_1^+)\sqrt{1+\gamma(R-2)}$ with increasing moment R and a change in the r and s amplitudes that corresponds to (9). This corresponds, for example, to allowance for the processes shown in Fig. 5e.

The expression (15) also makes it possible to calculate the isotopic variations of the mean-square charge radii. Note that the first two terms in (15) correspond to the mean-square charge radius of the even core (diagrams 1–3 in Fig. 4).

In the case of odd-neutron nuclei, there remain in (15) only the first, second, and fifth terms (diagrams 1–3, 7, and 8 in Fig. 4) and also the contribution due to the allowance for the Pauli principle and the zero-point shape vibrations.

If in (15) we go over to the f_{jk} representation, we readily find that the third and fourth terms (diagrams 4–6 of Fig. 4) correspond to the mean-square charge radius of the single-particle state in the deformed potential renormalized by the effect of the zero-point shape vibrations. At the same time, the fifth term (diagrams 7 and 8 in Fig. 4) is equivalent to the contribution to the mean-square charge radii from the change in the mean-square deformation. The remaining diagrams do not have analogs in the cranking model, but, as we shall see in what follows, they frequently play a fundamentally important role in the correct description of the changes in the mean-square charge radii associated with the structure of the states.

We note finally that in the method of approximate second quantization the mean number of particles will not be conserved if the superfluidity equations corresponding to (15) are not solved. However, this is extremely difficult to realize technically. But since we are interested in difference effects in the mean-square charge radii, this difficulty can be avoided by renormalizing the result obtained with allowance for the change in the mean number of nucleons. For this, it is necessary in the expression (15) to replace the single-particle radial integrals by the unit matrix, calculate the number of nucleons, and then renormalize.

Thus, after the description of the spectrum of excited states and the set of spectroscopic characteristics of the odd nucleus, our task is to calculate (15) with allowance for the

TABLE VII. Experimental and calculated values of $\mu(I)$, $Q(I)$, and $\Delta\langle r^2\rangle_{II'}$.

Nucleus	I^π	Q, e·b		μ, μ_{nuc}		$\Delta\langle r^2\rangle$, 10^{-3} F^2	
		Calculation	Experiment	Calculation	Experiment	Calculation	Experiment
^{73}Ge	9/2+	−0.367	−0.173(26)	−1.006	−0.879	12.1	27.4
	5/2+	−0.347	—	−0.445	−0.0941		
^{83}Kr	9/2+	0.228	0.270(13)	−0.957	−0.9707	22.8	12.8
	7/2+	0.269	0.459(6)	−0.983	−0.942(2)		
^{99}Tc	9/2+	−0.575	−0.34(34)	5.757	5.685	21.6	6.9
	7/2+	−0.146	—	4.756	3.6(9)		
^{119}Sn	1/2+	0	—	−1.442	−1.046	1.1	5.3
	3/2+	−0.091	−0.094(4)	0.892	0.633(3)		
^{121}Sb	5/2+	−0.493	−0.53(10)	3.940	3.360	−13.3	−5).8
	7/2+	−0.570	−0.37(8)	2.061	2.51(3)		
^{125}Te	1/2+	0	—	−1.301	−0.888	1.8	3.2
	3/2+	−0.262	−0.31(2)	0.806	0.604(5)		
^{127}I	5/2+	−0.688	−0.78	3.012	2.81	−9.6	−9.3
	7/2+	−0.655	−0.70	1.898	2.02		
^{129}I	7/2+	−0.539	−0.55(4)	2.211	2.621	15.0	13.7
	5/2+	−0.563	−0.68	3.355	2.81		
^{129}Xe	1/2+	0	—	−1.245	−0.778	2.7	5.4
	3/2+	−0.318	−0.41(6)	0.767	0.59(8)		
^{133}Cs	7/2+	−0.166	−0.0030(11)	2.001	2.582	10.9	5.6
	5/2+	−0.418	—	3.023	3.45(2)		
^{139}Xa	7/2+	0.057	0.21	2.119	2.778	10.3	9.6
	5/2+	−0.276	—	4.052			
^{141}Pr	5/2+	0.003	−0.0089(42)	4.187	4.136(2)	3.4	8.2
	7/2+	−0.076	—	2.366	2.8(2)		

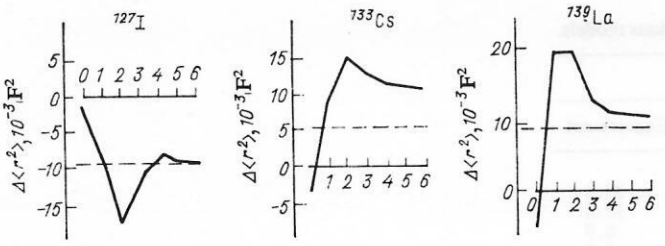

FIG. 6. Dependence of $\Delta\langle r^2\rangle_{cal}$ on the classes of diagrams in Fig. 4 taken into account in the calculation; the broken line represents the experiment.

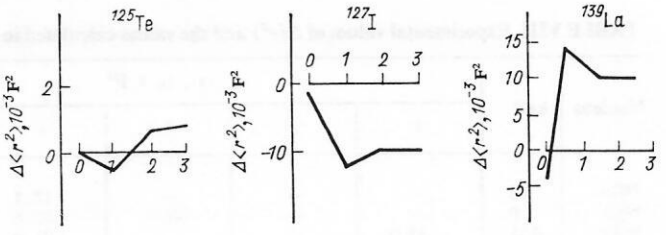

FIG. 8. Dependence of $\Delta\langle r^2\rangle_{cal}$ on the dynamical Pauli corrections: 1) calculation without allowance for them; 2) calculation with allowance for the first derivative; 3) with allowance for the first and second derivatives; 0) the single-particle model.

effect of the Pauli principle and the zero-point shape vibrations.

4. RESULTS OF CALCULATIONS OF $\Delta\langle r^2\rangle$ DUE TO EXCITATION OF THE NUCLEUS

Up to now, detailed calculations of Δ_1 have been made for spherical and transitional nuclei from ^{73}Ge to ^{141}Pr, in which it has been possible to achieve (see Sec. 3) a fairly good description of the excitation spectrum and the spectroscopic characteristics. We emphasize that all calculations were made in the approximation of an absolutely rigid average field, so that, using the deviations of the results of the calculations from the experimental data, it would be possible to draw conclusions about the nature of the rearrangement of the field following excitation of the nucleus.

Table VII gives the calculated and experimental spectroscopic characteristics of the lower part of the spectrum and the $\Delta\langle r^2\rangle$ of the spherical and transitional nuclei from ^{73}Ge to ^{141}Pr. It can be seen from the table that in the approximation of an absolutely rigid average field it is overall possible to describe reasonably well all the experimental data. For the most characteristic examples, we now consider the price at which such a description is achieved.

The part played by allowance for different classes of diagrams, the Pauli principle, and the zero-point shape vibrations

Figure 6 shows the dependence of $\Delta\langle r^2\rangle$ on the classes of diagrams for the nuclei ^{127}I, ^{133}Cs, ^{139}La. The number 0 corresponds to the single-particle model, and the number 1 indicates the contribution from the fragmentation of the single-particle states due to the coupling to the collective degrees of freedom (diagrams 4–6 in Fig. 4). The number 2 indicates the contribution to $\Delta\langle r^2\rangle$ from the phonon diagrams that corresponds to the change in the deformation parameter (diagrams 7 and 8 in Fig. 4). The numbers 3 and 4 correspond to the contribution of the linear diagrams, and the numbers 5 and 6 to the quadratic diagrams; these are without analogs in the cranking model and describe the static part of the effect of the Pauli principle.

It can be seen from the figure that all the classes of diagrams make a large contribution to $\Delta\langle r^2\rangle$, and not even one of them can be ignored. A large contribution to $\Delta\langle r^2\rangle$ is made by the classes of diagrams 1 and 2 in Fig. 6, and therefore in principle the cranking model makes it possible, by appropriate choice of the deformation parameter and the extension coefficient, to describe the observed value of $\Delta\langle r^2\rangle$ (see the caption to Fig. 1 in Sec. 2). But the real physics of the phenomenon remains hidden from us. It can also be seen from Fig. 6 that the classes of diagrams 5 and 6, quadratic in the collective amplitudes, make contributions to $\Delta\langle r^2\rangle$ smaller than the others. Thus, the calculations confirmed the results of the theoretical analysis which indicated that allowance for diagrams up to those quadratic in the collective amplitudes should make it possible to describe almost completely the structural part of the change in the mean-square charge radii following excitation of the nucleus.

Figures 7–9 show the dependence of $\Delta\langle r^2\rangle$ on the allowance made for zero-point shape vibrations of various multipolarity without allowance for the dynamical Pauli corrections, on the dynamical Pauli corrections without allowance for the zero-point shape vibrations (Fig. 8), and on the number of iterations (Fig. 9) in the solution of the integral equation (Fig. 5c). As can be seen from the figures, allowance for the effect of the zero-point shape vibrations up to multipolarity $\Lambda = 3$, the Pauli corrections up to the third derivative, and five or six iterations in the solution of the

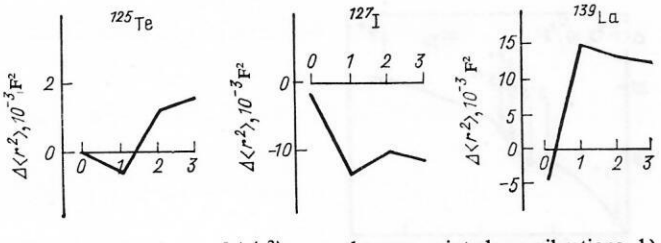

FIG. 7. Dependence of $\Delta\langle r^2\rangle_{cal}$ on the zero-point shape vibrations: 1) without allowance for them; 2) with allowance for those of quadrupole type; 3) with allowance for those of quadrupole and octupole type; 0) the single-particle model.

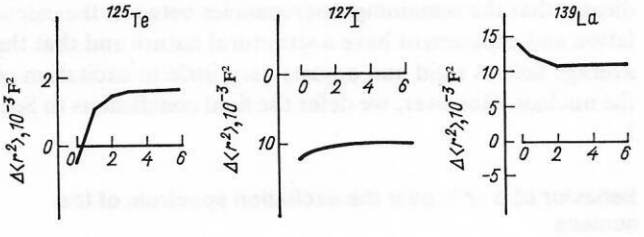

FIG. 9. Dependence of $\Delta\langle r^2\rangle_{cal}$ on the number of N of iterations in the solution of the equation of Fig. 5c.

TABLE VIII. Experimental values of $\Delta\langle r^2\rangle$ and the values calculated in various models.

Nucleus	keV	$\Delta\langle r^2\rangle$, 10^{-3} F^2				
		1	2	3	4	Experiment
^{73}Ge	13	—	—	—	12.1	27.4
^{83}Kr	9	—	—	33.0	22.8	12.8
^{99}Tc	141	—33.0	—	—	21.6	6.9
^{119}Sn	24	9.0	3.7	3.0	1.1	5.3
^{121}Sb	37	—	—	—	—13.3	—50.8
^{125}Te	36	—15.4	2.2	—3.0	1.8	3.2
^{127}I	59	—3.1	—68.0	—1.0	—9.6	—9.3
^{129}I	28	0.2	75.0	1.3	15.0	13.7
^{129}Xe	40	—	—	—	2.7	5.4
^{133}Cs	81	—3.0	30.0	1.0	10.9	5.6
^{139}La	166	—4.8	5.0	—	10.3	9.6
^{141}Pr	145	—	11.0	—	3.4	8.2

Note. 1) Single-particle model; 2) theory of finite Fermi systems; 3) model of Ref. 31; 4) present paper.

equation of Fig. 5c for the given class of diagrams effectively exhausts the possible effects. It can also be seen from Fig. 7 that allowance for the zero-point shape vibrations is extremely important, since at times it leads even to a change in the sign of $\Delta\langle r^2\rangle$. A large contribution to the value of $\Delta\langle r^2\rangle$ in strongly collective nuclei is made by allowance for the dynamical Pauli corrections associated with the change in the frequency of the collective modes (Fig. 8). Therefore, there is no point in making any calculations if they are not taken into account. We note that in odd-neutron nuclei, an odd proton being absent, there is no contribution to $\Delta\langle r^2\rangle$ from the static part of the Pauli principle (diagrams 9–16 in Fig. 4), and therefore the effects of the phonon rearrangement in these nuclei are most clearly expressed.

Comparison with the results of other models

Table VIII gives the results of calculations of $\Delta\langle r^2\rangle$ according to various nuclear models and compares them with experiment. It can be seen from the table that the single-particle model, which describes the structure of the states of odd nuclei very crudely, is frequently incapable of reproducing even the sign of the change in the mean-square charge radii. Though the calculations in the theory of finite Fermi systems and in Ref. 31 may agree with experiment, the agreement is only qualitative. But the DCM was able to reproduce rich spectroscopic information and, in the approximation of an absolutely rigid average field, to describe on the average the observed $\Delta\langle r^2\rangle$ values. Therefore, if the experimental data of Ref. 21 are taken as the "final truth," then the quantity $\Delta_2 = \Delta\langle r^2\rangle_{\text{exp}} - \Delta\langle r^2\rangle_{\text{cal}}$ has a random nature. This indicates that the remaining discrepancies between the calculation and experiment have a structural nature and that the average field is rigid and adjusts very little to excitation of the nucleus. However, we defer the final conclusions to Sec. 7.

Behavior of $\Delta\langle r^2\rangle$ over the excitation spectrum of the nucleus

To establish whether the average field is also stable at a high excitation energy, we made calculations of $\Delta\langle r^2\rangle$ over the spectrum of odd nuclei. Typical results of the calculations for the odd-neutron nucleus ^{125}Te are shown in Fig. 10. With increasing excitation energy, $\Delta\langle r^2\rangle$ increases, approximately reflecting the growth of the mean-square deformation.

It is important to note that up to an excitation energy of about 1 MeV the values of $\Delta\langle r^2\rangle$ remain of the same order as on transition of the nucleus from the first excited state to the ground state. This fact indicates that even at such a comparatively high excitation energy the average field of the nucleus remains fairly rigid and undergoes only a slight rearrangement.

5. MANIFESTATION OF COEXISTENCE OF THE SUPERFLUID AND NORMAL PHASES IN THE $\Delta\langle r^2\rangle$ VALUES OF ^{121}Sb

In the Sb nucleus, in which the spectrum of excited states is well described (see Fig. 3 and Table VII), there is observed to be an appreciable discrepancy with the experimental data[21] in the description of $\Delta\langle r^2\rangle$ between the $7/2^+$ first excited state and the $5/2^+$ ground state. It is important to note that in this case the result of the calculation depends weakly on the parametrization of the model, since the wave functions of the two states are close to single-particle states.

One could suppose that in this nucleus there is a strong rearrangement of the single-particle field on the transition from the ground to the excited state. But is it only due to rearrangement of the average field that such a change in the mean-square charge radius is observed? It is important to

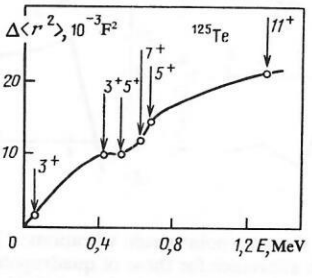

FIG. 10. Dependence of calculated $\Delta\langle r^2\rangle$ on the excitation energy of the ^{125}Te nucleus.

investigate other possible reasons of structural nature affecting $\Delta\langle r^2\rangle$.

Theory

The ground state of ^{121}Sb can be represented schematically as in Fig. 11a, but because pairing forces act between the nucleons a proton goes over from the $1d_{5/2}$ to the $2d_{5/2}$ level with formation of a pair on the Fermi surface and a hole in the $1/d_{5/2}$ state. At the same time, the core becomes a tellorium core (Fig. 11b), which is soft with a large value of the mean-square deformation and, therefore, a large mean-square charge radius. Therefore, even a small admixture of the superfluid phase in the ^{121}Sb ground state can lead to a large change in $\Delta\langle r^2\rangle$. Using the liquid-drop model, it is easy to estimate what contribution to $\Delta\langle r^2\rangle$ can be obtained by taking into account the admixture of the superfluid phase. Let R^2 be the mean-square charge radius of the ^{121}Sb ground state with Sn core and $\widetilde{R}^2$ be the corresponding quantity in the case of the Te core:

$$\left.\begin{aligned} R^2 &= \frac{3}{5}R_0^2\left(1+\frac{5}{4\pi}\beta^2\right)+\frac{1}{Z}r^2_{2d_{5/2}};\\ \widetilde{R}^2 &= \frac{3}{5}R_0^2\left(1+\frac{5}{4\pi}\widetilde{\beta}^2\right)+\frac{1}{Z}2r^2_{2d_{5/2}}-r^2_{1d_{5/2}}. \end{aligned}\right\} \tag{16}$$

In what follows, we shall use the tilde to identify the state with Te core. The single-particle radial integrals in (16) are, respectively, $r^2_{2d_{5/2}}=24.9\ \mathrm{F}^2$ $r^2_{1d_{5/2}}=19.6\ \mathrm{F}^2$, and experimentally[49] $\beta=-0.12$ and $\widetilde{\beta}=0.20$. Therefore, the difference between the mean-square charge radii is $\widetilde{R}^2-R^2=0.334\ \mathrm{F}^2$, and if the admixture of the superfluid phase is $\sim 1\%$, then the increase in the mean-square charge radius of the ground state will be $3.34\times10^{-3}\ \mathrm{F}^2$. However, such a calculation does not take into account the important coupling to the collective states of the Te core.

The total wave function of the $5/2^+$ state can be represented schematically as in Fig. 11. But in the $7/2^+$ state an admixture of the superfluid phase does not arise, since in the lower part of the single-particle spectrum there is no analog of the $1g_{7/2}$ level. It is readily seen that an appreciable effect from an admixture of the superfluid phase is to be expected in nuclei whose neighbors have strongly differing collective properties.

To calculate the admixture of the superfluid phase, it is necessary to calculate the spectrum of ^{121}Sb particle states with Sn core and the spectrum of hole states with Te core and take into account their mixing through nondiagonal pairing forces. The wave functions of these states have the form

$$|5/2^+_1\rangle=\Sigma F^{(1)}_{jR}D^+_j\alpha_{nj}|\,\mathrm{Sn}\rangle_R,\quad |\widetilde{5/2^+_i}\rangle=\Sigma\widetilde{F}^{(i)}_{jR}\widetilde{D}^+_j\alpha_{n'j}|\,\mathrm{Te}\rangle_R.$$

We write the total wave function as

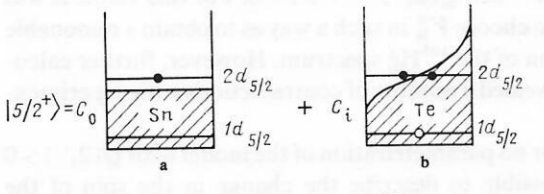

FIG. 11. Schematic representation of the ^{121}Sb wave function.

$$|5/2^+\rangle=C_0|5/2^+_1\rangle+\Sigma\widetilde{C}_i|\widetilde{5/2^+_i}\rangle, \tag{17}$$

where the summation is over all states with Te core. The coefficients C_0 and $\widetilde{C}_i$ and the energy of the $5/2^+$ state with allowance for the admixture of the superfluid phase can be readily calculated:

$$C_0^2=\left(1+\Sigma\frac{V_i^2}{(\widetilde{E}_i-E)^2}\right)^{-1},$$

$$\widetilde{C}_i=-C_0\frac{V_i}{\widetilde{E}_i-E},\quad E=E_0-\Sigma\frac{V_i^2}{\widetilde{E}_i-E}. \tag{18}$$

Here, $\widetilde{E}_1$ is the energy of the ith state with Te core, E_0 is the energy of the $5/2^+_1$ state with Sn core, and V_i is the matrix element of the interaction between the first solution with Sn core and the ith solution with Te core:

$$V_i=\langle 5/2^+_1|\,\hat{V}_{\mathrm{nd}}\,|\widetilde{5/2^+_i}\rangle, \tag{19}$$

where

$$\hat{V}_{\mathrm{nd}}=-G\Sigma(-1)^{j_1-m_1+j_2-m_2}a^+_{n_1j_1m_1}a^+_{n_2j_1-m_1}a_{n_3j_2-m_2}a_{n_4j_2m_2}. \tag{20}$$

Here, a^+_{njm} is the operator of creation of a particle in the state with quantum numbers njm. Note that the expression (20) has been represented in a form that separates explicitly states with different principal quantum numbers. Going over in (20) to quasiparticles by a Bogolyubov transformation and substituting the resulting expression in (19), we obtain the required matrix element of the interaction,

$$V_i=2G\sum_{j_1R}F^{(1)}_{j_1R}\widetilde{F}^{(i)}_{j_1R}D_{j_1}\widetilde{D}_{j_1}\sum_{j_2}(2j_2+1)$$
$$\times u_{j_2}\widetilde{v}_{j_2}(u_{j_2}\widetilde{u}_{j_2}+v_{j_2}\widetilde{v}_{j_2})^{j_2-1/2}\prod_{j\neq j_2}(u_j\widetilde{u}_j+v_j\widetilde{v}_j)^{j+1/2}, \tag{21}$$

and the mean-square radius of the ^{121}Sb ground state with the wave function (17) is

$$\langle R^2\rangle=C_0^2\langle r^2\rangle+\Sigma\widetilde{C}_i^2\langle\widetilde{r}^2_i\rangle+2C_0\Sigma\langle\mathrm{Sn}|\,\hat{R}^2\,|\mathrm{Te}\rangle C_i, \tag{22}$$

where $\langle\tilde{r}^2_0\rangle$ and $\langle r^2_i\rangle$ are calculated by the method explained in Sec. 3, and $\hat{R}^2$ is the operator (11). The matrix element $\hat{R}^2_n=\langle\mathrm{Sn}|R^2|\mathrm{Te}\rangle$ in the expression (22) is calculated in the same way as in Sec. 3, but it must be borne in mind that the superfluidity coefficients for different cores are different.

Thus, finding the first solution of Eq. (18), we can use (22) to find the mean-square charge radius of the $5/2^+$ state of ^{121}Sb with allowance for the admixture of the superfluid phase, and the calculated $\Delta\langle r^2\rangle_{7/2^+,5/2^+}$.

Results of the calculations

The calculations showed that the admixture of the superfluid phase is very small and in sum is 1.09% for all the hole solutions with Te core. Nevertheless, the increase in the mean-square charge radius of the $5/2^+$ ground state of ^{121}Sb due to the influence of the admixture of the superfluid phase produced by the nondiagonal pairing is $9.2\times10^{-3}\ \mathrm{F}^2$. The differences between the mean-square charge radii with Sn and Te cores for solutions with greater energy are greater than the limit given by the liquid-drop model. This indicates

TABLE IX. Experimental values of $\Delta\langle r^2\rangle$ for the ^{121}Sb isotope and values calculated in various approximations.

$\Delta\langle r^2\rangle$, 10^{-3} F^2			
Calculation		Experiment	
1	2	Ref. 21	Ref. 20
−13.3	−22.5	−50.8	−24.6

Note. 1) Without allowance for admixture of the superfluid phase; 2) complete calculation.

that the effects due to the coupling of the collective and single-particle degrees of freedom make a large contribution to the mean-square charge radii.

Table IX give the calculated $\Delta\langle r^2\rangle$ without allowance for the admixture of the superfluid phase, with allowance for it, and the experimental values taken from Refs. 20 and 21. As can be seen from the table, the contribution to $\Delta\langle r^2\rangle$ from the admixture of the superfluid phase is of the same order as the main effect. Therefore, in nuclei having even neighbors with very different collective properties the calculations must be made with allowance for the influence of the admixture of the superfluid phase. It can also be seen from Table IX that the result of the complete calculation agrees reasonably well with the experimental value of Ref. 20, whose authors, however, point out that the error may be large. Therefore, the uncertainty in the experimental data on $\Delta\langle r^2\rangle$ at present make it impossible to draw any conclusions about the possible nature of the "observed" discrepancy.

6. NATURE OF THE ISOTOPIC EFFECTS IN THE CHARGE RADII OF $^{183-199}$Hg AND $^{127-137}$Cs

Whereas the change in the mean-square charge radius of a nucleus following excitation can be divided into a structural part and a part associated with rearrangement of the average field, in the case of the isotopic variations of the mean-square charge radii this cannot be done in explicit form, since the population numbers change by one or two nucleons for neighboring isotopes. Therefore, the information about the nature of the effective nuclear forces is here masked to a greater extent. Nevertheless, the isotopic dependences of the mean-square charge radii manifest interesting features of the nuclear dynamics, and their study is of independent interest.

The isotopes $^{183-198}$Hg

The large changes in the mean-square charge radii discovered not all that long ago[24,25] in the isotopes of mercury on the transition from the isotopes with A equal to 186 and 184 to the nuclei with A equal to 185 and 183, respectively, stimulated intensive theoretical study of this question in the framework of the cranking model.[50,51] The results of these investigations can be formulated as follows: In contrast to the even–even isotopes of mercury, in which the ground state has an oblate equilibrium shape with small mean-square deformation β^2, in the odd isotopes with A equal to 183 and 185 the ground state has a prolate shape with large β^2. This must lead to a sharp increase in the mean-square charge radius on the transition from the even to the odd isotopes. Thus, the experimentally observed even–odd jumps in the mean-square charge radii of the neutron-deficient isotopes of mercury were attributed to the coexistence in the excitation spectra of these nuclei of states with different equilibrium shapes.

This phenomenon has long attracted the interest of the experimentalists. But despite great exertions, for example, in the excitation spectra of the barium isotopes, it has not proved possible to discover states with different equilibrium shapes, although all calculations predicted their appearance at a low excitation energy.[52,53] In this situation it was usually said that the calculations are, of course, approximate, since they do not take into account possible γ instability of the nucleus and the second minimum in the total energy need not be a real minimum on the β, γ plane. The situation in the mercury isotopes could be just the same, although in the even isotopes there was a kind of detection[54] of a low-lying band of states with $K^\pi = 0^+$, this band corresponding to a prolate shape with large β^2.

However, in recent years states of nuclei usually regarded as shape isomers have been successfully described in the framework of the DCM after careful examination of the part played by the blocking effect in the formation of collective modes.[55] It is therefore of great interest to describe the observed jump in the mean-square charge radii of the mercury isotopes in the framework of the DCM.

Excitation spectra and spectroscopic characteristics. In the considered case of the mercury isotopes, the $Q(2_1^+)$ values are not known at all, while $B(E2, 0^+\to 2^+)$ are known only in two nuclei; from them the mass parameter B_2 was determined, while $\varkappa$ was determined from the condition of best description of the spectrum of the ^{195}Hg isotope and was the same for all the remaining nuclei. Turning to the calculations, we began by taking $Q(2_1^+)$ for the even isotopes in accordance with the results of the calculations in the cranking model,[56] i.e., $Q(2_1^+) \sim +0.5$ e·b. For this value, it was possible to choose V_{ls}^n in such a way as to obtain a reasonable description of the ^{193}Hg spectrum. However, further calculations revealed a number of contradictions with experimental facts:

1. For no parametrization of the model with $Q(2_1^+) > 0$ was it possible to describe the change in the spin of the ground state, $3/2^- \leftrightarrow 1/2^-$, in the nuclei with $A = 195, 185,$

TABLE X. Experimental values and the values used in the calculations for the collective parameters and the constant of the spin–orbit forces for the Hg and Cs nuclei.

Nucleus	A	V_{ls}	$E(2_1^+)$, MeV	$E(3_1^-)$, MeV	Q, e·b (calculation)	$B(E2,\ 0^+ \to 2^+)$, $e^2 \cdot b^2$	
						calculation	experiment
Hg	183	0.125	0.300	1.386	−1.65	1.78	—
	185	0.125	0.367	1.410	−1.60	1.60	1.95 (45)
	187	0.125	0.405	1.428	−1.09	1.25	1.40 (25)
	189	0.125	0.413	1.424	−0.81	1.06	—
	191	0.125	0.416	1.416	−0.80	1.04	—
	193	0.125	0.423	1.412	−0.80	1.03	—
	195	0.125	0.428	1.407	−0.80	1.02	—
Cs	127	0.185	0.388	1.946	−1.03	0.64	0.781 (50)
	129	0.185	0.443	1.949	−0.87	0.47	0.69 (5)
	131	1.190	0.536	2.009	−0.48	0.47	1.00 (8)
	133	0.195	0.667	2.153	−0.19	0.39	0.44 (3)
	135	0.205	0.847	2.417	−0.08	0.20	—
	137	0.215	1.313	3.275	−0.06	0.12	—

183. The $1/2^-$ state always remained an excited state with energy of order 150 keV.

2. The sign of the quadrupole moment of the $3/2^-$ state in the ^{193}Hg isotope was not reproduced.

3. The second $3/2^-$, $5/2^-$ solutions were found at a rather high excitation energy, in disagreement with experiment.

4. In the light mercury isotopes, the $13/2^+$ level became the ground state, and not $1/2^-$, as experimentally.

One might imagine that the failure to describe the excitation spectra of the mercury isotopes with $Q(2_1^+) > 0$ in the framework of the DCM is due to the fact that, in contrast to the light and intermediate nuclei from ^{83}Kr to ^{141}Pr, where the model describes the properties of the excitation spectra well, new, as yet unknown features of the nuclear dynamics are manifested in heavy nuclei. However, we believe that there are no grounds for accepting the calculations in the cranking model, which gives $Q(2_1^+) > 0$, since within its framework one obtains a good description of neither the excitation spectra nor the spectroscopic characteristics. Moreover, the early calculations of the mean-square charge radii,[57] in contradiction to the subsequent experiments, also predicted a jump of λ in the even isotopes of mercury with $A \leqslant 186$.

Analyzing the excitation spectra of the odd isotopes of platinum, for which the quadrupole moments of the even nuclei are well known, we established that the constant V_{ls}^n must be fairly small if the single-particle $2f_{5/2}$ state is to be a hole state. In such a case, a band of states can be formed with $\Delta I = 2$ ($5/2^-$, $9/2^-$, . . .), for which there are experimental indications. But for small V_{ls}^n in the light mercury isotopes the band with $\Delta I = 2$ based on $13/2^+$ observed experimentally can be formed only if the core has a negative quadrupole moment. Changing the sign of the quadrupole moment and fixing its magnitude by fitting to the splitting between the $19/2^+$ and $21/2^+$ states in ^{195}Hg, and taking in small constant $V_{ls}^n = 0.125$, we found that one can obtain a complete description of the excitation spectrum of this nucleus. Moreover, for unchanged parameters of the model calculations of the other nuclei completely reproduced the experimental picture of the changes in the properties of the odd mercury isotopes. This is the most weighty evidence that the effective quadrupole moment of the "particle + core" system with $Z = 80$ has the negative sign.

In Table X we give the values of $\varkappa$ and B_2, converted to $Q(2_1^+)$ and $B(E2)$, as used in the calculations for the even

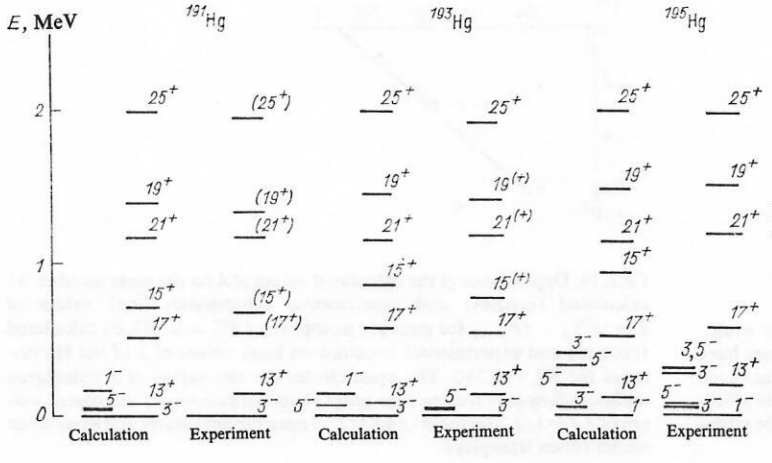

FIG. 12. Calculated and experimental spectra of the mercury isotopes (the spin values have been doubles).

TABLE XI. Experimental and calculated spectroscopic characteristics of low-lying states of the Hg and Cs isotopes.

Nucleus	A	I^π	E, keV		μ, μ_{nuc}		Q, $e\cdot b$	
			Calculation	Calculation	Experiment	Experiment	Calculation	Experiment
Hg	183	$1/2^-$	0	0	0.519	0.524 (5)	0	—
	185	$1/2^-$	0	0	0.515	0.507 (4)	0	—
	187	$3/2^-$	0	0	−1.062	−0.593 (4)	−0.530	−0.50 (23)
	189	$3/2^-$	0	0	−1.167	−0.6086	−0.257	−1.15 (25)
	191	$3/2^-$	0	0	−1.170	—	−0.332	−0.41 (41)
		$3/2^-$	0	0	−1.183	−0.6276	−0.225	−0.86 (38)
	193	$13/2^+$	113	141	−1.236	−1.0584	−0.766	±1.08 (10)
		$1/2^-$	0	0	0.514	0.5415	0	—
	195	$13/2^+$	141	176	−1.247	−1.0446	−0.854	±1,27 (11)
Cs	127	$1/2^+$	0	0	1.998	1.46 (2)	0	—
	129	$1/2^+$	0	0	2.106	1.482 (9)	0	—
		$5/2^+$	0	0	2.876	3.543 (2)	−0.424	−0.620 (6)
	131	$5/2^+$	232	134	2.264	1.98 (13)	−0.145	—
		$7/2^+$	0	0	2.001	2.5820	−0.166	−0.003 (1)
	133	$5/2^+$	18	81	3.023	3.45 (2)	−0.418	—
		$5/2^+$	256	161	2.075	1.48 (50)	−0.089	—
	135	$7/2^+$	0	0	2.105	2.7324	−0.122	0.050 (2)
	137	$7/2^+$	0	0	2.133	2.8413	−0.082	0.051 (1)

mercury isotopes. For the experimental values, see Refs. 58 and 59. Figure 12 shows how one can in the framework of the DCM describe the spectra of the excited states of the best studied mercury isotopes. It can be seen that the calculations excellently reproduce the experimentally observed changes in the properties of the excitation spectrum with decreasing mass number. The extent to which one can also describe the spectroscopic characteristics can be seen from Table XI.

What is decisive in the formation of such excitation spectra? It is the renormalization of the effective forces by the zero-point shape vibrations. This is illustrated by Fig. 13, which presents calculations in various approximations. It can be seen that allowance for the zero-point vibrations up to multipolarity $\Lambda = 3$ is exhaustive.

Charge radii. We recall that the general expression for the charge radius of an odd-neutron nucleus is equivalent to allowance for the processes shown in Fig. 4 (diagrams 1–3, 7, and 8). We note that the result will depend not only on the way in which the neutron Fermi surface, which determines the form of the excitation spectrum, is structured but also on the shape of the proton Fermi surface, since the summation in (15) in the case of an odd-neutron nucleus is also over the proton states.

The results of the calculations showed that for the stan-

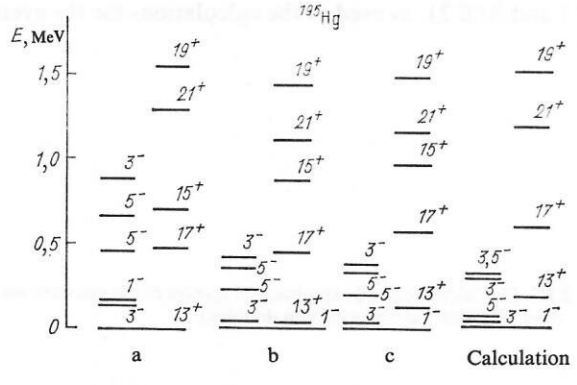

FIG. 13. Influence of zero-point shape vibrations of different multipolarities on the formation of the ^{195}Hg spectrum. The spin values have been doubled. a) Calculation without allowance for the zero-point shape vibrations; b) calculation with allowance for only the quadrupole vibrations; c) calculation with allowance for quadrupole and octupole vibrations.

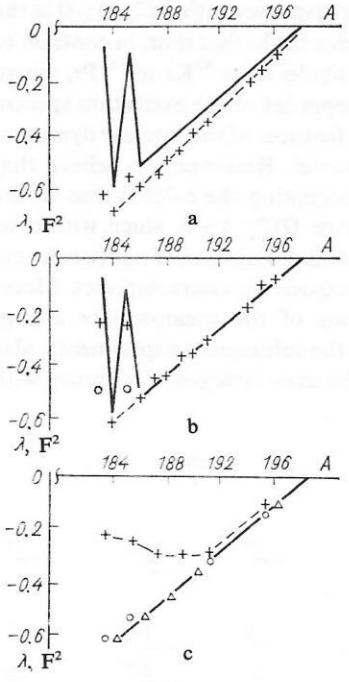

FIG. 14. Dependence of the calculated values of λ on the mass number: a) calculated (crosses) and experimental (continuous line) values of $\lambda = \langle r^2\rangle_A - \langle r^2\rangle_{198}$ for mercury isotopes and $V_{ls}^p = 0.287$; b) calculated (crosses) and experimental (continuous line) values of λ of the Hg isotopes for $V_{ls}^p = 0.310$. The open circles are the values of λ calculated without allowance for the zero-point shape vibrations; c) calculated values of λ for $1/2^-$ (crosses) and $3/2^-$ (open circles) states and even–even nuclei (open triangles).

dard parametrization of the proton Fermi surface $V_{ls}^{p} = 0.287$ the isotopic dependence has a slope different from the experimental one; see Fig. 14a. The isotopic slope could be reproduced by choosing $V_{ls}^{p} = 0.310$. One then automatically obtained a description of the jump in the charge radii of the isotopes with $A = 183$ and 185, as shown in Fig. 14b. One could imagine that the abrupt increase in the charge radius of the $1/2^-$ state, which in the isotopes with $A = 183$ and 185 becomes the ground state, is due to the sharp increase in the mean-square deviation, but this is not so. If one leaves out the contribution of the zero-point shape vibrations in the renormalization of the single-particle radial integrals, leaving them as purely single-particle integrals, the result is greatly changed and almost no jump at all is observed in the mean-square charge radii (Fig. 14b, crosses), although the value of β^2 remains almost unchanged.

Thus, the sharp increase of the charge radius in the mercury isotopes with $A = 183$ and 185 is due to the fact that the $1/2^-$ state, which becomes the ground state in these nuclei, has a large effective charge but not a large value of β^2, as assumed earlier. This is illustrated in Fig. 14c, which shows the dependence of λ on A for the $1/2^-$ and $3/2^-$ states and for the even nuclei. It can be seen from the figure that the charge radius of the $1/2^-$ state increases monotonically on the interval $A \leqslant 187$ as compared with the $3/2^-$ mean-square charge radius and the values for the even nuclei. And when $1/2^-$ becomes the ground state, an abrupt jump is observed.

A few words about the isotopic slope. Previously, it had not been described by any of the calculations, and this had suggested[60] a compressibility of nuclear matter. But it follows from our calculations that there is no need to speak of compressibility at all. The slope is associated with correct description of the proton Fermi surface and, thus, with correct description of the charge mean-square deformation.

The isotopes $^{127-137}$Cs

Although the experimentally observed bends in the isotopic dependence of the mean-square charge radii of the cesium isotopes[22] are not so striking as in the mercury isotopes, study of the odd-proton nuclei is of great interest, since in this case all diagram classes contribute to the value of the mean-square charge radius. In addition, in odd-proton nuclei the excitation spectra, spectroscopic characteristics, and mean-square charge radii are related to the shape of only the proton Fermi surface.

Excitation spectra and spectroscopic characteristics. Table X gives the $Q(2_1^+)$ and $B(E2)$ values of the even cores in a comparison with experiment and the constants V_{l2} of the spin–orbit forces for the cesium isotopes with $A = 127$–137. Also given are the experimental energies of the 2_1^+ states and the energies of the 3_1^- states of the corresponding xenon cores calculated by the method of Ref. 47.

As for the mercury isotopes, the calculations took into account all the single-particle states in the energy interval from -25 to $+10$ MeV, this making it possible to take into account more fully the influence of the octupole zero-point shape vibrations on the formation of the excitation spectra and the values of the mean-square charge radii.

Figure 15 gives the calculated and experimental spectra of the cesium isotopes with $A = 127$–137. The calculations

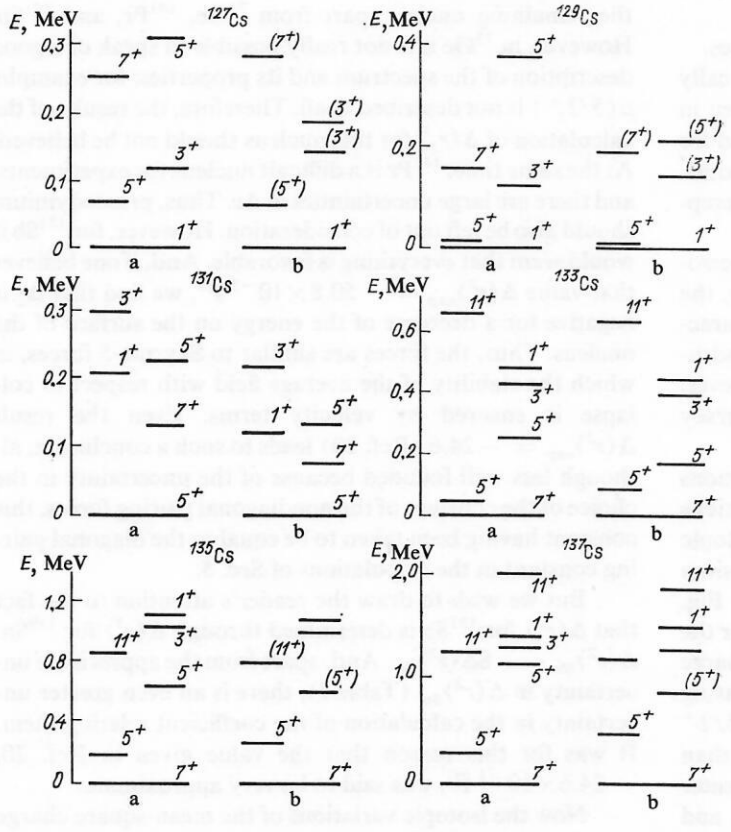

FIG. 15. Calculated and experimental spectra of the cesium isotopes. The spin values have been doubled. a) calculation; b) experiment.

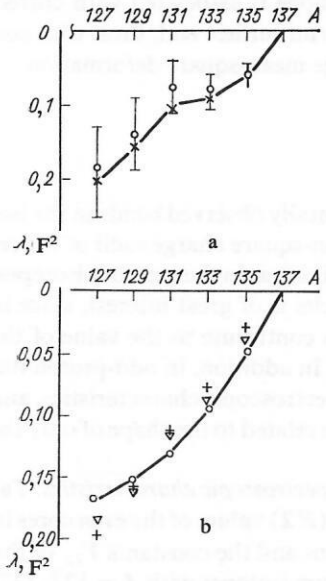

FIG. 16. Dependence of calculated values of λ on the mass number: a) calculated (crosses) and experimental values of $\lambda = \langle r^2\rangle_A - \langle r^2\rangle_{137}$ for the ground states of the Cs isotopes; b) calculated values of λ for the $1/2_1^+$ (crosses), $5/2_1^+$ (inverted open triangles), and $7/2_1^+$ (open circles) states of the Cs isotopes.

reproduce well all the main features of the spectra:

1. The change in the spin of the ground state, $7/2^+ \rightarrow 5/2^+$ and $5/2^+ \rightarrow 1/2^+$, on the transition from the isotopes with $A = 133$ to $A = 131$ and from $A = 131$ to $A = 129$, respectively.

2. The lowering of the energy of the $5/2_2^+$ state as the mass number is decreased to 131, followed, however, by an increase with further decrease in A.

3. The narrowing of the intervals between the states.

We note, however, that the calculations systematically overestimate the energies of the $3/2_2^+$ states (not given in Fig. 15); their positions cannot be correctly reproduced for any of the isotopes or for any parametrization of the model. A special study is here needed, especially since the discrepancy is systematic.

Table XI gives the calculated and experimental spectroscopic characteristics of the cesium isotopes. Basically, the calculations reproduce quite well the spectroscopic characteristics, although in ^{137}Cs and ^{135}Cs the sign of the quadrupole moment of the ground state is not described. However, its value is too small and does not come within the accuracy of description of the quadrupole moment in the DCM.

Charge radii. Figure 16a gives the results of calculations of λ and a comparison with experiment. The calculations reproduce the experimentally observed bends in the isotopic dependence of the mean-square charge radii of the cesium isotopes. The nature of this phenomenon is shown in Fig. 16b, which gives λ as a function of the mass number for the $1/2^+$, $5/2^+$, and $7/2^+$ states. It can be seen that the charge radii of these states decrease monotonically with decreasing mass number. The mean-square charge radii of the $5/2^+$ states in the isotopes with $A = 131$–137 are greater than those of the $7/2^+$ states, the reason for this being the greater admixture of collective modes in the wave function, and therefore on the transition from ^{133}Cs to ^{131}Cs, when the $5/2^+$ state becomes the ground state, a decrease of the mean-square charge radius is hardly observed.

As the mass number is decreased, a single-phonon configuration on a $2d_{5/2}$ single-quasiparticle level becomes the main component of the $1/2^+$ state. But the Pauli principle causes the frequency of the phonon to increase, and the contribution to the mean-square charge radius from the phonon decreases, in contrast to the case when the total spin is $5/2^+$. This has the consequence that with decreasing mass number the mean-square charge radius of the $1/2^+$ state actually becomes smaller than that of the $5/2^+$ state, and for this reason a bend is observed in the isotopic dependence when the $1/2^+$ state becomes the ground state (transition from $A = 131$ to $A = 129$). However, the large experimental error makes it impossible to see this phenomenon.

7. DISCUSSION OF THE RESULTS

We turn to Table VII, from which it can be seen that for the nuclei ^{83}Kr, ^{99}Tc, and ^{133}Cs the results of the calculations of $\Delta\langle r^2\rangle$ significantly exceed the experimental values *despite all their uncertainty* (Table I). And since excitation of these nuclei causes the density at their surface to increase, Δ_2 is negative for all three nuclei. We thus arrive at the conclusion that the effective forces acting between the nucleons in the nuclei are similar to Skyrme-3 forces, in which the stability of the average field is ensured by a strong density dependence induced by the three-particle forces. If the $\Delta\langle r^2\rangle_{\text{exp}}$ data of Ref. 21 are regarded as not absolute but on an equal footing with the others (see Table I), the conclusion drawn above *does not contradict* the results of the calculations for the remaining nuclei, apart from ^{73}Ge, ^{141}Pr, and ^{121}Sb. However, in ^{73}Ge it is not really possible to speak of a good description of the spectrum and its properties; for example, $\mu(5/2_1^+)$ is not described at all. Therefore, the results of the calculation of $\Delta\langle r_2\rangle$ for this nucleus should not be believed. At the same time, ^{141}Pr is a difficult nucleus for experiments, and there are large uncertainties in Δv. Thus, praseodymium should also be left out of consideration. However, for ^{121}Sb it would seem that everything is favorable. And, if one believes that value $\Delta\langle r^2\rangle_{\text{exp}} = -50.8\times10^{-3}$ F^2, we find that Δ_2 is negative for a decrease of the energy on the surface of the nucleus. Thus, the forces are similar to Skyrme-5 forces, in which the stability of the average field with respect to collapse is ensured by velocity terms. Even the result $\Delta\langle r^2\rangle_{\text{exp}} = -24.6$ (Ref. 20) leads to such a conclusion, although less well founded because of the uncertainty in the choice of the constant of the nondiagonal pairing forces, this constant having been taken to be equal to the diagonal pairing constant in the calculations of Sec. 5.

But we wish to draw the reader's attention to the fact that $\Delta\langle r^2\rangle$ for ^{121}Sb is determined through $\Delta\langle r^2\rangle$ for ^{119}Sn: $\Delta\langle r^2\rangle_{\text{Sb}} \sim -8\Delta\langle r^2\rangle_{\text{Sn}}$. And, apart from the appreciable uncertainty in $\Delta\langle r^2\rangle_{\text{Sn}}$ (Table I), there is an even greater uncertainty in the calculation of the coefficient relating them. It was for this reason that the value given in Ref. 20, -24.6×10^{-3} F^2, was said to be very approximate.

Now the isotopic variations of the mean-square charge

radii. The conclusion that the effective forces in nuclei are like Skyrme-3 forces agrees with the choice in the DCM of the value $R_0 = 1.25A^{1/3}$ for the 50%-decrease radius of the average field. However, the large contributions of the structure effects and their frequently strong dependence on the way in which the proton Fermi surface is constructed necessitate a considerable extension of the number of studied nuclei before conclusions can be more definite.

CONCLUSIONS

The approach considered here to the study of the variations in the mean-square charge radii of nuclei as a result of their excitation as well as in the isotopic dependences already makes it possible at the present stage, despite all the uncertainty in the experimental information, to draw certain conclusions about the nature of the effective nuclear forces. Namely, preference must be given to the forces for which the stability (against collapse) of the single-particle field which they generate is ensured by a strong dependence on the density. But further advance in discriminating between the various effective nuclear forces is impossible without reliable experimental information on $\Delta\langle r^2\rangle$.

[1]V. I. Kuprikov and V. E. Mitroshin, Preprint No. 667 [in Russian], Leningrad Institute of Nuclear Physics (1981).
[2]V. I. Goldanskii and R. H. Herber, *Chemical Applications of Mössbauer Spectroscopy*, Academic Press, New York (1968).
[3]V. S. Shpinel', *Rezonans gamma-lucheĭ v kristallakh* (*Resonances of Gamma Rays in Crystals*), Nauka, Moscow (1969).
[4]H. Frauenfelder, *The Mössbauer Effect*, Benjamin, New York (1962) (Russian translation published by Atomizdat, Moscow (1964)).
[5]G. K. Wertheim, Mössbauer Effect: *Principles and Applications*, Academic Press, New York (1964) (Russian translation published by Mir, Moscow (1966)).
[6]J. Danon, *Lectures of the Mössbauer Effect*, Gordon and Breach, New York (1968).
[7]G. Bhide, *Mössbauer Effect and its Applications*, McGraw-Hill, New York (1973).
[8]N. W. Greenwood and T. C. Gibb, *Mössbauer Spectroscopy*, Chapman and Hall, London (1971).
[9]S. G. Cohen and M. Pasternak, *Perspectives in Mössbauer Spectroscopy*, Plenum Press, New York (1973).
[10]U. Gonser, *Mössbauer Spectroscopy*, Springer-Verlag, Berlin (1976).
[11]R. L. Cohen, *Applications of Mössbauer Spectroscopy*, Vol. 1, Plenum Press, New York (1973).
[12]G. K. Shenoy and F. E. Wagner (eds.), Mössbauer *Isomer Shifts*, North-Holland, Amsterdam (1978).
[13]P. Gutlich, L. Reiner, and A. Trautwein, *Mössbauer Spectroscopy and Transition Metal Chemistry*, Vol. 10, Heldelberg-Verlag, Berlin (1978), p. 280.
[14]P. H. Barret *et al.*, Phys. Rev. B **12**, 1676 (1975).
[15]H. Miclitz and J. Litterst, Phys. Rev. Lett. **33**, 480 (1974).
[16]P. A. Montano *et al.*, Phys. Rev. **178**, 1, 6 (1978).
[17]K. V. Makaryunas, R. A. Kalinauskas, and K. I. Davidonis, Zh. Eksp. Teor. Fiz. **60**, 1569 (1971) [Sov. Phys. JETP **33**, 848 (1971)].
[18]P. Rueysegger and W. Kündig, Helv. Phys. Acta **46**, 165 (1973).
[19]P. Roggwiller and W. Kündig, Phys. Rev. B **11**, 4179 (1975).
[20]G. M. Kalvius and G. K. Shenoy, At. Data Nucl. Data Tables **14**, 639 (1974).
[21]Zh. I. Adymov *et al.*, in: *Tezisy dokladov XXXII soveshchaniya po yadernoĭ spektroskopii i strukture atomnogo yadra* (*Abstracts of Papers at the 32nd Symposium on Nuclear Spectroscopy and Nuclear Structure*), Kiev (1982), p. 549.
[22]S. Ullrich and E. W. Otten, Nucl. Phys. **A248**, 173 (1975).
[23]P. B. Russel *et al.*, Nucl. Phys. **A210**, 133 (1973).
[24]J. Bonn, G. Huber, H.-J. Kluge *et al.*, Phys. Lett. **38B**, 308 (1972).
[25]J. Bonn *et al.*, Z. Phys. A **276**, 203 (1976).
[26]T. Kühl *et al.*, Phys. Rev. Lett. **39**, 180 (1977).
[27]P. A. Shirley, Rev. Mod. Phys. **36**, 339 (1964).
[28]L. M. Dautov, in: *Tezisy XXIII soveshchaniya po yadernoĭ spektroskopii i strukture atomnogo yadra* (*Abstracts of Papers at the 23rd Symposium on Nuclear Spectroscopy and Nuclear Structure*), Tbilisi (1973), p. 228.
[29]L. M. Dautov *et al.*, in *Proc. of the Intern. Conf. on Mössbauer Spectroscopy*, Bratislava (1973), pp. 3, 619.
[30]L. M. Dautov *et al.*, Preprint P-8 [in Russian], Institute of Nuclear Physics, Kazakh Academy of Sciences, Alma-Ata (1976).
[31]R. A. Uher and R. A. Sorensen, Nucl. Phys. **86**, 2 (1966).
[32]V. A. Belyakov, Zh. Eksp. Teor. Fiz. **49**, 832 (1965) [Sov. Phys. JETP **22**, 578 (1966)].
[33]L. M. Dautov *et al.*, Preprint P-2 [in Russian], Institute of Nuclear Physics, Kazakh Academy of Sciences, Alma-Ata (1978).
[34]R. N. Kasymbalinov and E. E. Sapershteĭn, Yad. Fiz. **35**, 1489 (1982) [Sov. J. Nucl. Phys. **35**, 871 (1982)].
[35]R. N. Kasymbalinov *et al.*, Yad. Fiz. **40**, 397 (1984) [Sov. J. Nucl. Phys. **40**, 252 (1984)].
[36]J. Speth, Nucl. Phys. **A135**, 445 (1969).
[37]J. Meyer and J. Speth, Phys. Lett. **39B**, 330 (1972).
[38]V. G. Soloviev, Phys. Lett. **21**, 311 (1966).
[39]W. Stepien-Rudzka, Acta Phys. Pol. **B2**, 583 (1971).
[40]V. E. Mitroshin, Preprint No. 441 [in Russian], Leningrad Institute of Nuclear Physics (1978).
[41]V. E. Mitroshin, Izv. Akad. Nauk SSSR, Ser. Fiz. **38**, 2074 (1974).
[42]E. I. Erokhina and V. E. Mitroshin, Izv. Akad. Nauk SSSR, Ser. Fiz. **45**, 37 (1981).
[43]V. S. Zvonov and V. E. Mitroshin, Izv. Akad. Nauk SSSR, Ser. Fiz. **42**, 2 (1978).
[44]V. E. Mitroshin, Izv. Akad. Nauk SSSR, Ser. Fiz. **44**, 986 (1980).
[45]V. S. Zvonov and V. E. Mitroshin, Izv. Akad. Nauk SSSR, Ser. Fiz. **44**, 65 (1980).
[46]V. E. Mitroshin, Preprint No. 563 [in Russian], Leningrad Institute of Nuclear Physics (1980).
[47]V. G. Solov'ev, *Teoriya slozhnykh yader*, Nauka, Moscow (1971); English translation: *Theory of Complex Nuclei*, Pergamon Press, Oxford (1976).
[48]A. Bohr and B. R. Mottelson, Nuclear Structure, Vol. 1, Benjamin, New York (1969) (Russian translation published by Mir, Moscow (1971)).
[49]G. B. Krygin and V. E. Mitroshin, Preprint No. 924 [in Russian], Leningrad Institute of Nuclear Physics (1984).
[50]S. Frauendorf and V. V. Pashkevich, Phys. Lett. **55B**, 365 (1975).
[51]F. Dickmann and K. Deitrich, Z. Phys. **263**, 211 (1973).
[52]T. W. Colon and A. J. Elwyn, Nucl. Phys. **142**, 359 (1970).
[53]G. F. Brinkman and L. Myunkhov, Fiz. Elem. Chastits At. Yadra **3**, 366 (1972) [Sov. J. Part. Nucl. **3**, 189 (1972)].
[54]D. Proetel *et al.*, Phys. Lett. **31**, 896 (1973).
[55]O. D. Kovrigin and V. E. Mitroshin, Preprint No. 666 [in Russian], Leningrad Institute of Nuclear Physics (1981).
[56]R. V. Jolos, Preprint R4-9357 [in Russian], JINR, Dubna (1975).
[57]D. Colb and C. Y. Wong, Nucl. Phys. **A245**, 205 (1975).
[58]N. Rud, D. Ward *et al.*, Phys. Rev. Lett. **31**, 1421 (1973).
[59]D. Proetel *et al.*, Phys. Lett. **48B**, 102 (1974).
[60]V. A. Karnaukhov and L. A. Petrov, *Yadre, udalennye ot linii beta-stabil'nosti* (*Nuclear Far from the Line of Beta Stability*), Énergoizdat, Moscow (1981).
[61]C. M. Lederer *et al.*, *Tables of Isotopes*, Wiley, New York (1978).
[62]V. Paar, Nucl. Phys. **A211**, 29 (1971).

Translated by Julian B. Barbour